Molecular Plant
Research Article

CellPress
PARTNER JOURNAL

TOLs Function as Ubiquitin Receptors in the Early Steps of the ESCRT Pathway in Higher Plants

Jeanette Moulinier-Anzola[1,4], Maximilian Schwihla[1,4], Lucinda De-Araújo[1,2,4], Christina Artner[1,3], Lisa Jörg[1], Nataliia Konstantinova[1], Christian Luschnig[1] and Barbara Korbei[1,*]

[1]Institute of Molecular Plant Biology, Department of Applied Genetics and Cell Biology, University of Natural Resources and Life Sciences, Vienna (BOKU), Muthgasse 18, 1190 Vienna, Austria

[2]Present address: Department of Molecular Toxicology and Environment, Biotechnology Center-Eduardo Mondlane University, Av. de Mocambique, Km 1.5. Maputo, Mozambique

[3]Present address: Institute of Science and Technology Austria (IST Austria), Am Campus 1, 3400 Klosterneuburg, Austria

[4]These authors contributed equally to this article.

***Correspondence: Barbara Korbei (barbara.korbei@boku.ac.at)**

https://doi.org/10.1016/j.molp.2020.02.012

ABSTRACT

Protein abundance and localization at the plasma membrane (PM) shapes plant development and mediates adaptation to changing environmental conditions. It is regulated by ubiquitination, a post-translational modification crucial for the proper sorting of endocytosed PM proteins to the vacuole for subsequent degradation. To understand the significance and the variety of roles played by this reversible modification, the function of ubiquitin receptors, which translate the ubiquitin signature into a cellular response, needs to be elucidated. In this study, we show that TOL (TOM1-like) proteins function in plants as multivalent ubiquitin receptors, governing ubiquitinated cargo delivery to the vacuole via the conserved Endosomal Sorting Complex Required for Transport (ESCRT) pathway. TOL2 and TOL6 interact with components of the ESCRT machinery and bind to K63-linked ubiquitin via two tandemly arranged conserved ubiquitin-binding domains. Mutation of these domains results not only in a loss of ubiquitin binding but also altered localization, abolishing TOL6 ubiquitin receptor activity. Function and localization of TOL6 is itself regulated by ubiquitination, whereby TOL6 ubiquitination potentially modulates degradation of PM-localized cargoes, assisting in the fine-tuning of the delicate interplay between protein recycling and downregulation. Taken together, our findings demonstrate the function and regulation of a ubiquitin receptor that mediates vacuolar degradation of PM proteins in higher plants.

Key words: ubiquitination, ESCRT pathway, ubiquitin receptor, plasma membrane protein degradation

Moulinier-Anzola J., Schwihla M., De-Araújo L., Artner C., Jörg L., Konstantinova N., Luschnig C., and Korbei B. (2020). TOLs Function as Ubiquitin Receptors in the Early Steps of the ESCRT Pathway in Higher Plants. Mol. Plant. **13**, 717–731.

INTRODUCTION

The covalent modification of a protein by ubiquitin, or ubiquitination, modulates responses to ever-changing environmental conditions as well as numerous aspects of plant development. This type of post-translational modification is associated with all three major protein degradation pathways—the proteasome, the vacuole/lysosome, and the autophagosome—where it helps control the half-life of proteins (Clague and Urbe, 2010; Korbei and Luschnig, 2013; Zientara-Rytter and Sirko, 2016), but also affects localization, activity, and interactions of many proteins (Komander and Rape, 2012). Ubiquitin conjugation is extraordinarily complex in plants, with more than 1500 ubiquitin–protein ligases actively participating in this process (Hua and Vierstra, 2011). Substrates can be mono-ubiquitinated, multiple mono-ubiquitinated, or poly-ubiquitinated, whereby ubiquitin can form linear or branched chains by means of linkage to the N terminus or internal lysine residues (K6, K11, K27, K29, K33, K48, and K63) of other ubiquitin moieties (Husnjak and Dikic, 2012). Thus, a large diversity in ubiquitination types exists, each thought to affect protein fate in a specific manner (Komander and Rape, 2012). Decoding of

Published by the Molecular Plant Shanghai Editorial Office in association with Cell Press, an imprint of Elsevier Inc., on behalf of CSPB and IPPE, CAS.

such signals is accomplished by ubiquitin-binding domain (UBD)-containing proteins, or ubiquitin receptors, that non-covalently associate with ubiquitin. UBDs are typically short amino acid stretches that display a low binding affinity toward ubiquitin and do not have a strict consensus sequence (Husnjak and Dikic, 2012). They function as crucial switches in the integration of different stimuli, allowing for regulated participation of the proteins containing them in different networks. Whereas the importance of ubiquitination in plants is unequivocal and recently several studies strived to unravel the ubiquitome of plants (Svozil et al., 2014; Johnson and Vert, 2016; Walton et al., 2016; Aguilar-Hernandez et al., 2017), a full grasp of the significance and the variety of roles played by this modification can only be reached by understanding the function of ubiquitin receptors, which translate the ubiquitin signature into a cellular response.

The sole presence of ubiquitin on plasma membrane (PM) cargo appears to be a sufficient signal to initiate its sorting (Herberth et al., 2012; Martins et al., 2015), with both mono- and K63-linked poly-ubiquination implicated in endocytic trafficking of PM proteins into the vacuolar lumen for degradation (Lauwers et al., 2010; Erpapazoglou et al., 2014; Piper et al., 2014). The *trans*-Golgi network, which acts as an early endosome in plants (Dettmer et al., 2006), receives the endocytosed cargo. From there, it is either recycled back to the PM or further delivered to the vacuole via a series of multi-protein complexes, the Endosomal Sorting Complex Required for Transport (ESCRT) machinery, which binds and sequesters ubiquitinated proteins and ushers them into the intraluminal vesicles (ILVs) of multi-vesicular bodies (MVBs) (Paez Valencia et al., 2016; Gao et al., 2017; Isono and Kalinowska, 2017). Cargo recognition and concentration largely depends on ESCRT-0 while other ESCRT components function to promote membrane bending and scission (Hurley and Hanson, 2010). Several ESCRTs have subunits with UBDs, which serve in anchoring the ubiquitinated cargoes and guiding them through the endocytic degradation route (Hurley, 2010).

Plants contain orthologs of most of the ESCRT proteins but lack canonical ESCRT-0 subunits (Winter and Hauser, 2006). Plant-specific substitutes for this subunit could be several ubiquitin receptors in the early endocytic pathway of plants (Mosesso et al., 2019). In *Arabidopsis* the conserved scaffolding protein, apoptosis-linked gene-2 interacting protein X (ALIX), binds membranes, ubiquitin, and K63-linked ubiquitin chains, and interacts with Vacuolar Sorting Protein 23A (VPS23A) and FYVE1 (Fab1, YOTB, Vac1, and EEA1)/FREE1 (FYVE DOMAIN PROTEIN REQUIRED FOR ENDOSOMAL SORTING 1), essential for ESCRT-I as well as ESCRT-III function (Cardona-Lopez et al., 2015; Kalinowska et al., 2015; Shen et al., 2018). The plant-specific FYVE1/FREE1 localizes to MVBs and binds ubiquitin as well as PtdIns(3)P, and furthermore interacts with the Src homology-3 (SH3) domain-containing protein 2 (SH3P2), VPS23A/B, and the ESCRT-III complex (Barberon et al., 2014; Gao et al., 2014; Kolb et al., 2015; Belda-Palazon et al., 2016). At the PM, the ubiquitin-binding protein SH3P2 has been implicated in vacuolar trafficking of ubiquitinated cargoes, as it binds K63-linked ubiquitin and VPS23A and localizes to clathrin-coated vesicles (Kolb et al., 2015; Nagel et al., 2017). Target of Myb 1 (TOM1) proteins are evolutionarily ancient ubiquitin receptors, which function in the capturing of ubiquitinated cargo and are thought to act together with or replace the ESCRT-0 machinery (Wang et al., 2010). In plants, this type of ubiquitin adaptor has greatly expanded, resulting in nine TOM1-like (TOL) proteins that harbor all functionally relevant features for the recognition and sorting of ubiquitinated cargoes close to or at the PM (Korbei et al., 2013). TOLs bind ubiquitin *in vitro* and localize to the PM as well as early endosomal structures (Korbei et al., 2013). A higher-order *tol* loss-of-function mutant combination shows defects in endosomal cargo trafficking and severe defects in plant development, indicating that TOLs are indeed essential for degradation of PM proteins (Korbei et al., 2013).

Only few ubiquitin receptors functioning in the vacuolar degradation pathway of plants have so far been characterized (Spitzer et al., 2006; Gao et al., 2014; Kalinowska et al., 2015; Nagel et al., 2017; Wang et al., 2017), and the functionality of their UBDs and their regulation have not been assessed. Eukaryotic PM-borne ubiquitin receptors that have been reported, such as E/ANTH endocytic receptors, do not contain conserved UBDs in plants (Holstein and Oliviusson, 2005), indicating that ubiquitinated cargoes need to be recognized by other PM-localized ubiquitin receptors (Korbei et al., 2013; Nagel et al., 2017). According to our findings, members of the TOL protein family can function as multivalent ubiquitin receptors in the first steps of ESCRT-mediated protein degradation, ensuring cargo delivery to the vacuole. TOL2 and TOL6, residing in the cytosol, at the PM, and in early endosomes, bind to K63-linked ubiquitin via two tandemly arranged conserved UBDs. Function and localization of TOLs appear to be regulated by ubiquitin binding and ubiquitination, whereby the ubiquitin receptor's own ubiquitination affects its ability to assist in the degradation of ubiquitinated cargo, potentially by influencing localization of the receptor protein. Our analysis thus provides insights into the functioning of PM cargo recognition in plants by a ubiquitin receptor protein.

RESULTS

TOLs Function in the Degradation of Ubiquitinated Proteins and Show Various Subcellular Localizations

TolQ plants, lacking five out of the nine TOLs (*TOL2*, *TOL3*, *TOL5*, *TOL6*, and *TOL9*), are characterized by pleiotrophic, strong developmental defects and show impaired vacuolar degradation of several PM proteins without obvious general defects in endocytosis (Korbei et al., 2013; Yoshinari et al., 2018). Defective endosomal sorting, associated with mutations in ESCRT subunits, is notorious for triggering ubiquitinated protein accumulation, due to their impaired degradation in the vacuole (Kalinowska and Isono, 2014; Kolb et al., 2015). Consequently, to establish the involvement of the TOLs, not just for individual cargoes but on a global scale, we analyzed the total amount of ubiquitin conjugates in *tolQ* and compared them with wild-type cell lysates (Figure 1A and 1B). Both 6-day-old seedlings and adult leaves from *tolQ* plants accumulated ubiquitinated proteins at a much higher level than their wild-type counterparts (Figure 1A and 1B, top panel). For a statistical evaluation, we compared total signal intensities in the ubiquitin blot of the respective lysates normalized with either the tubulin signal (Figure 1A, bottom panel) or the Coomassie signal (Figure 1B, bottom lane) and found a significant increase in the normalized signal corresponding to total ubiquitination in *tolQ*

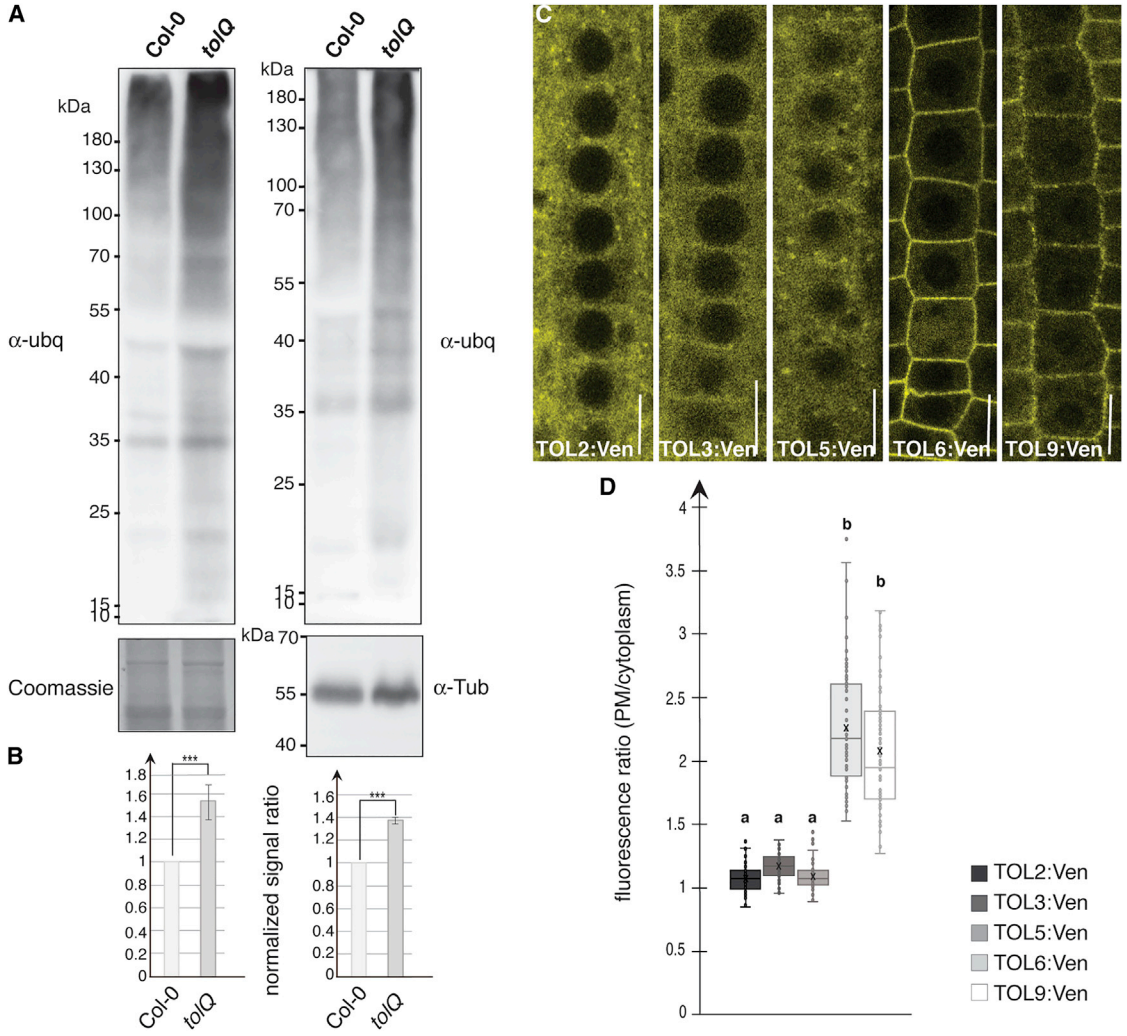

Figure 1. TOLs Function in Degradation of Ubiquitinated Proteins and Show Differential Localization.

(A) Accumulation of ubiquitin (ubq) conjugates in *tolQ* mutants. Total protein extracts of adult leaves of 21-day-old plants (left panels) or 6-day-old seedlings (right panels) of Col-0 (wild type) and *tolQ* plant lines were subjected to SDS–PAGE and immunoblotting using an anti-ubq antibody (top panels, α-ubq) or as a loading control, Coomassie staining (left bottom panel) for the total leaf extract or an anti-tubulin antibody (right bottom panel, α-Tub) for the seedlings.

(B) Statistical evaluation of differences in the signal intensities of the ubiquitination patterns in Col-0 or *tolQ* lysates of 21-day-old adult leaves (left graph) or seedlings (right graph). Average gray values in areas of identical size and shape of total lanes were determined and normalized to the average gray values either of the entire lane of the corresponding Coomassie brilliant blue staining signal (left graph) or to the corresponding tubulin signals (right graph). The resulting normalized signal ratios between Col-0 and *tolQ* are presented as means ± SD ($n = 3$ biological replicates) analyzed by one-way ANOVA with post hoc Tukey HSD test (***$p \leq 0.001$).

(C) Signal distribution in root epidermal meristem cells of 6-day-old plants expressing *TOL2p*::*TOL2*:*Venus*, *TOL3p*::*TOL3*:*Venus*, *TOL5p*::*TOL5*:*Venus*, *TOL6p*::*TOL6*:*Venus*, and *TOL9p*::*TOL9*:*Venus* in the respective *tol single* mutant background. Scale bars, 10 μm.

(D) Relative signal intensities (signal at PM normalized to signal intensities in cytoplasm) of TOL2:Ven, TOL3:Ven, TOL5:Ven, TOL6:Ven, or TOL9:Ven in respective single-mutant *tol* root meristem cells (73–86 root epidermal cells for each dataset from three independent biological repeats) were analyzed by one-way ANOVA with post hoc Tukey HSD test. The different letters above each bar indicate statistically significant differences ($p \leq 0.01$).

with respect to the wild-type signal. Thus, plants lacking a significant proportion of TOL activity show a wide-ranging defect in the turnover of ubiquitinated proteins, indicating that respective TOLs are required for proper degradation of ubiquitinated substrates.

Although TOLs function redundantly, as single *tol* mutant plant lines show no obvious phenotype, there is evidence for a certain diversification in the function of the TOLs, as TOL6 has been found to function at the PM in the degradation of PIN2 (Korbei et al., 2013), whereas TOL5, functions at MVBs, where it co-localizes with BOR1 on its route to the vacuole under high-boron conditions (Yoshinari et al., 2018). We therefore cloned five *TOL* expression cassettes, composed of *TOL* cDNA constructs expressed under their own promoter, into binary vectors with C-terminal Venus (Ven) tags. These constructs were transformed into corresponding single-knockout *tol* plant lines (Korbei et al., 2013), and the fusion

proteins were tested for expression and correct size (Supplemental Figure 1).

The analysis of the subcellular localization of different TOLs by confocal laser scanning microscopy (CLSM) revealed that in epidermal root cells of *tol2-1 TOL2p*::*TOL2*:*Ven*, *tol3-1 TOL3p*::*TO32*:*Ven*, and *tol5-1 TOL5p*::*TOL5*:*Ven* seedlings, the Venus signal was mostly cytoplasmic with punctate signals, potentially representing accumulations in endosomal structures (Figure 1C, three left panels), as previously shown for *tol5-1 TOL5p*::*TOL5*:*mCherry*, which is also found in endocytic membrane fractions (Korbei et al., 2013). TOL6:Ven and TOL9:Ven signal showed a pronounced accumulation close to or at the PM (Figure 1C, two right panels). These differences in localization of Venus-tagged TOL reporter lines is statistically highly significant (Figure 1D), indicating that proteins within the TOL family show activity at different subcellular sites. We therefore decided to focus on one member of the cytosolic TOLs, namely TOL2, and one member of the more PM-localized TOLs, namely TOL6, in our further analysis to elicit potential redundancies and differences within the TOL protein family.

TOL6 Interacts and Co-localizes with the ESCRT-I Subunit VPS23A

We have previously demonstrated that TOLs act in early steps of ubiquitinated PM protein degradation in higher plants (Korbei et al., 2013), but experimental evidence linking TOL function to ESCRT-dependent protein sorting has been absent so far. We therefore investigated whether TOLs interact with ESCRT-I, which function as a first downstream receptor for ubiquitinated PM cargo (Gao et al., 2017; Isono and Kalinowska, 2017) We chose VPS23A (VPS23.1/ELC), which is the *Arabidopsis* homolog of the mammalian and yeast subunits responsible for ESCRT-0 binding (Bache et al., 2003; Katzmann et al., 2003), binds ubiquitin, and associates with other ESCRT-I subunits to form a putatively intact plant ESCRT-I complex (Spitzer et al., 2006). Co-localization studies between a VPS23A:RFP reporter line (Nagel et al., 2017) and Venus-tagged TOL2 (TOL2:Ven; Figure 2A) as well as TOL6 (TOL6:Ven; Figure 2B) showed overlaps in signal distribution. Furthermore, VPS23A:RFP as well as TOL6 is found in early endosomal structures (Korbei et al., 2013; Nagel et al., 2017) where they co-localize (Figure 2C).

To further manifest this interaction, we attempted *in vivo* co-precipitation of the two TOLs with VPS23A. We therefore probed the cell lysate of plant lines expressing TOL2:Ven in *tol2-1* background (Figure 2D, middle panel) with beads coupled with glutathione *S-transferase (*GST)-tagged VPS23A. Here, a clear difference can be seen when precipitating with the VPS23A coupled beads, whereby TOL2:Ven is co-precipitated while essentially no TOL2:Ven signal is found when GST-coupled beads are used (Figure 2D, top panel).

Apart from pull-down experiments, we performed a yeast mating-based split-ubiquitin system assay (Stagljar et al., 1998). In these assays, both TOL2 and TOL6 were found to interact with full-length VPS23A as well as with both the C-terminal and N-terminal portions of VPS23A (Supplemental Figure 2A–2C). In another set of *in vitro* experiments, full-length bacterially expressed and purified TOL2 and TOL6 (Figure 2E, Input, top panel) specifically bound to VPS23A (Figure 2E, PD, top panel) coupled to glutathione beads, while only unspecific binding was detected to GST-coupled glutathione beads (Figure 2E, PD, top panel). We performed additional *in vitro* binding assays with C-terminal and N-terminal portions of VPS23A both N-terminally tagged with GST, whereby TOL2 and TOL6 interacted with both VPS23A constructs (Supplemental Figure 3A, TOL2 and B TOL6).

Further evidence for functional crosstalk between VPS23A and TOLs came from co-expression analyses, by employing Genevestigator 7.0.1 (Hruz et al., 2008), revealing a strong correlation in the expression of the two genes (Supplemental Figure 3C). Together, our *in vitro* and *in vivo* interaction assays provide support for a scenario in which TOL2 and TOL6 act in conjunction with canonical elements of the ESCRT sorting machinery.

TOL2 and TOL6 Bind the Ubiquitin, with a Preference for K63-Linked Ubiquitin Chains

TOL2 and TOL6, which bind to ubiquitin *in vitro* (Korbei et al., 2013), both possess two N-terminally located UBDs, the VHS and GAT domains, highly conserved in all TOL proteins. To assess whether these TOLs show linkage-specific preferences for specific ubiquitin chains, we performed *in vitro* binding assays. We used His-tagged, bacterially expressed and purified full-length versions of TOL2 and TOL6 (Figure 3A) as well as a GST-tagged truncated version of TOL6, comprising only the two N-terminal UBDs (GST:N-term.TOL6; Supplemental Figure 4A and 4B). Equal amounts of di-ubiquitin (Figure 3A and Supplemental Figure 4B), with different linkage—linear, K48-linked, which is relatively compact or K63-linked, which adopts an open conformation (Tenno et al., 2004; Varadan et al., 2004)—were added to beads coupled with equal amounts of His-tagged TOL2, TOL6, or GST:N-term.TOL6 (Figure 3A and Supplemental Figure 4B, bottom panels). Presence of the tandemly arranged UBDs seemed to provide a strong bias for binding to K63-linked ubiquitin chains, since all three constructs showed a strikingly higher preference to precipitate K63-linked di-ubiquitin (Figure 3A and Supplemental Figure 4B). Such stronger binding to K63-linked ubiquitin chains is consistent with several studies in which certain tandem UBDs permit the preferential recognition of K63-linked ubiquitin chains (Sims and Cohen, 2009; Lange et al., 2012).

TOL6 Binds the Ubiquitin via Two N-Terminal UBDs

The N-terminal VHS domain, consisting of eight α helices arranged in a superhelix (Hong et al., 2009), was demonstrated to function in intracellular protein-sorting processes (Lohi et al., 2002; Bonifacino, 2004) and is followed by an ~150-residue GAT domain, which adopts a three-helix bundle structure (Prag et al., 2007). Earlier, we demonstrated that the TOLs bind directly to ubiquitin and that a mutation of ubiquitin at position isoleucine 44 to an alanine (I44A) reduced protein binding (Korbei et al., 2013). This suggested that this binding occurs via known UBDs, as many of those characterized interact with the hydrophobic patch of ubiquitin, centered around I44 (Husnjak and Dikic, 2012). The functional significance of UBDs predicted in TOL proteins is, however, unknown.

To characterize the TOL VHS and GAT domains, we mutagenized conserved amino acids in these two domains in an effort to create

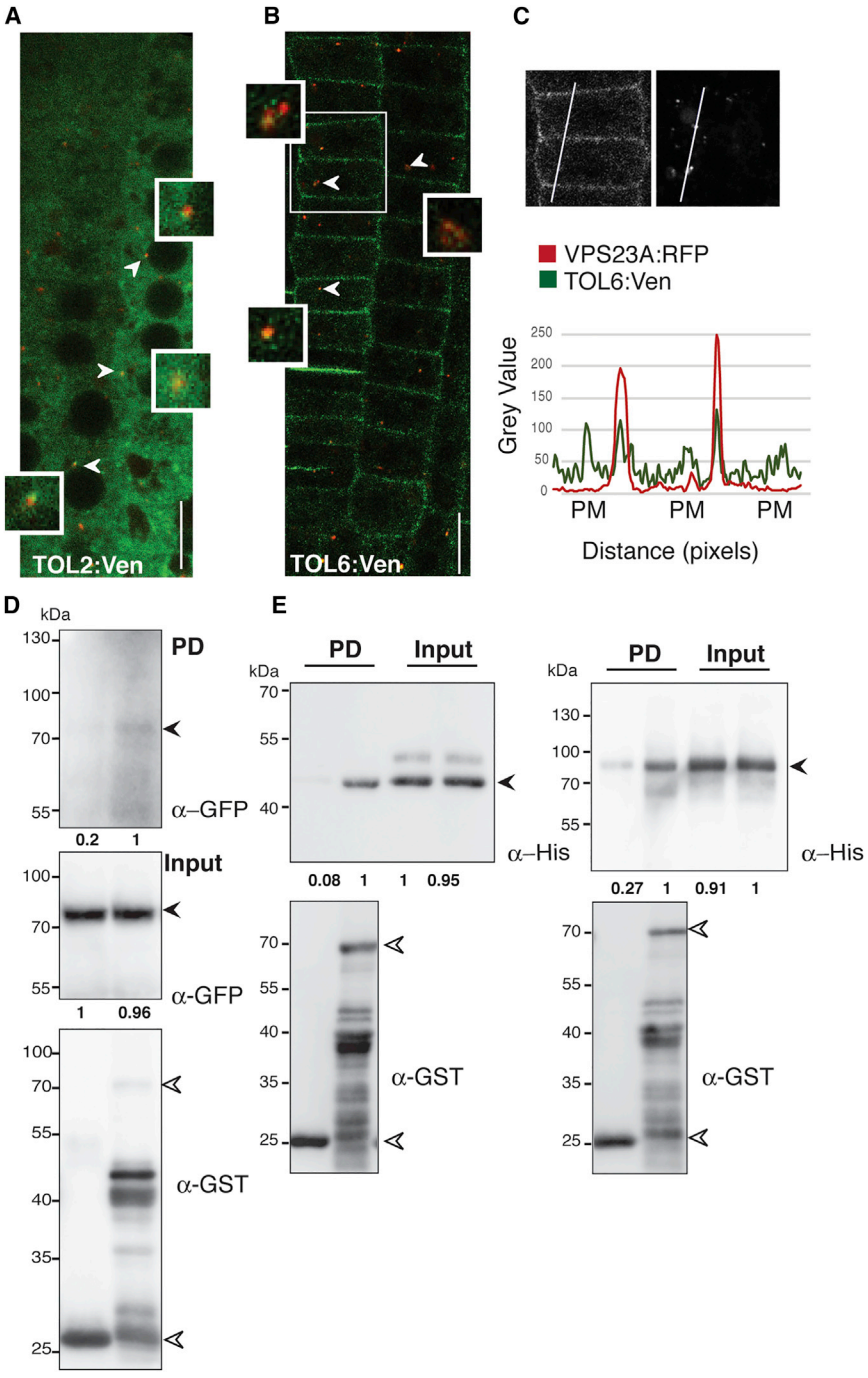

Figure 2. TOL6 Functions in the ESCRT Pathway.

(A and B) Co-localization of TOL2:Ven (**A**, green) and TOL6:Ven (**B**, green) with VPS23A:RFP (VPS23.1-TagRFP [Nagel et al., 2017], red) in root epidermis cells of 6-day-old seedlings was analyzed using CLSM. Arrowheads indicate co-localization of reporter signals, which are enlarged (4×) in small panels next to arrowheads. Scale bars, 10 μm.

(C) The top panel shows the enlarged image of the boxed area in **(B)** but separated into the two channels, with TOL6:Ven shown on the left and VPS23A:RFP on the right. The graph below shows the profiles of Ven (Venus; green) and RFP (red) signal intensity along a straight line, which were acquired by ImageJ. The PM areas are indicated.

(D) Co-precipitation of TOL2 with VPS23A. Bead-bound GST:VPS23A (70 kDa) and GST alone (26 kDa) as control (bottom panel, open arrowheads) were used to precipitate TOL2:Ven (top panel, arrowhead) out of total plant lysates of *TOL2p*::*TOL2*:*Venus* in *tol2-1* 7-day-old seedlings (middle panel, arrowhead). Bead-bound materials were analyzed by immunoblotting with anti-GFP (α-GFP) antibody. TOL2:Ven (pull-down [PD]; top panel, arrowhead) clearly co-precipitated with VPS23A while no binding can be seen to GST-tagged beads.

(E) Bead-bound full-length GST:VPS23A, or GST alone (open arrowheads, bottom panel) were incubated with equal amounts of TOL2:6xHis (44 kDa, arrowhead, Input, top left panel) or TOL6:6xHis (76 kDa, arrowhead, Input, top right panel). After washing, bead-bound materials were analyzed by immunoblotting with anti-His (α-His) antibodies. TOL2 (PD, left panel) and TOL6 (PD, right panel) clearly bind VPS23A while no binding can be seen to GST-tagged beads.

Normalized signal intensities are indicated below blots and the strongest signal in each experiment was arbitrarily set to 1.

a *TOL* allele deficient in ubiquitin binding. Analysis of the VHS domain of human STAM proteins highlighted the importance of a tryptophan at position 26 (W26) (Hong et al., 2009). Furthermore, an asparagine (N) in the α4 helix of the VHS domain of STAM2 was found to be a highly conserved residue, pivotal to ubiquitin binding (Lange et al., 2012). When we aligned different VHS domains of mammals and plants we found these amino acids to be conserved in all nine TOL proteins (Supplemental Figure 4D) and therefore mutated them in TOL6 (corresponding to W25 and N73) by site-directed mutagenesis to alanine, yielding the mutant allele *tol6*^{W25A,N73A} = *tol6* ^{mVHS} (Figure 3B).

The GAT domain was found to contain two conserved motifs (Bilodeau et al., 2004), where sequence alignment of different GAT domains showed that the first, formed by the α1 helix, is conserved in all TOL proteins (Supplemental Figure 4D), while the second located in the α3 helix (Bilodeau et al., 2004) is also conserved, albeit not as stringently. We thus focused on the first motif, which also caused stronger defects in ubiquitin binding when mutated in a human GAT domain (Bilodeau et al., 2004), and performed site-directed mutagenesis of DLL (246–248) to AAA and DML (250–252) to AAA in *TOL6*, obtaining *tol6* ^{mGAT} (Figure 3A). Finally, a combination of the mutations introduced into *TOL6* VHS and GAT domains resulted in the *tol6*^{mTOTAL} allele (Figure 3A).

The ability of the mutant *tol* alleles to bind ubiquitin *in vitro* was assessed by pull-down assays. Equal amounts of glutathione beads linked to purified bacterially expressed GST-tagged

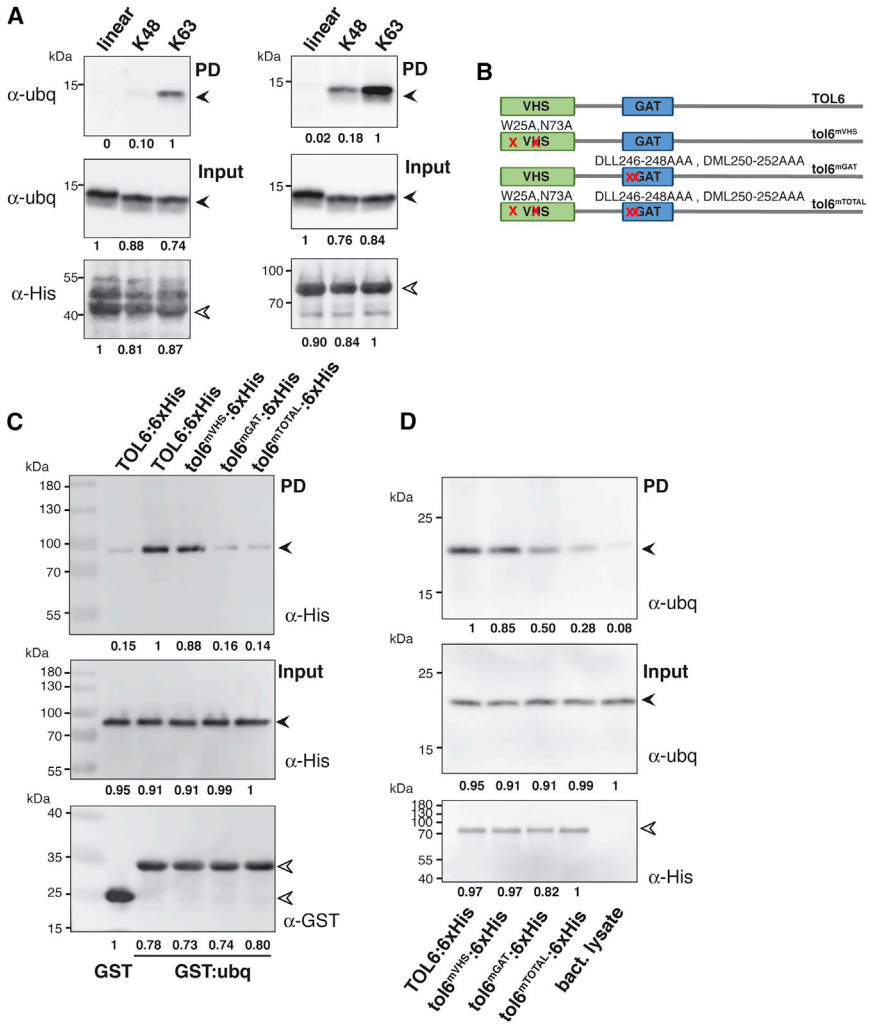

Figure 3. Mutation of the UBDs of TOL6 Abrogates Its Ubiquitin-Binding Ability.

(A) Di-ubiquitin-binding assay with recombinant TOL2:6xHis (44 kDa, left panel) or TOL6:6xHis (76 kDa, right panel). Equal amounts of linear, K48-linked (K48), or K63-linked (K63) di-ubiquitin (arrowhead, middle panels) were added to equal amounts of bead-bound TOL2:6xHis (open arrowhead, left bottom panel) and TOL6:6xHis (open arrowhead, right bottom panel). After precipitation, the binding of di-ubiquitin to TOL2:6xHis (arrowhead, top left panel) or TOL6:6xHis (arrowhead, top right panel) was analyzed by immunoblotting with anti-ubq antibody (α-ubq). While a strong band can be seen for K63-linked di-ubiquitin, there is only a weaker band for K48-linked di-ubiquitin detected (17 kDa, arrowhead, top panel). The P4D1 antibody we used showed an equal partiality to all three di-ubiquitins (Supplemental Figure 4C).

(B) Schematic representation of the TOL6 constructs used. VHS (green box) and GAT (blue box); mutated amino acids are designated by a red "x".

(C) Ubiquitin-binding assay. Equal amounts of bead-bound GST or GST:ubq (26 kDa or 34.5 kDa, respectively, open arrowhead, bottom panel) were incubated with equal amounts of TOL6 constructs (TOL6:6xHis or tol6:6xHis, 75 kDa, arrowhead, middle panel, probed with anti His-antibody, α-His). Precipitated proteins were probed with α-His (top panel). While TOL6-6xHis and tol6^{mVHS}:6xHis clearly co-precipitate with GST:ubq, tol6^{mGAT}:6xHis and tol6^{mTOTAL}:6xHis do not. There is no co-precipitation of TOL6-6xHis with GST-bound beads alone (arrowhead, top panel).

(D) Di-ubiquitin-binding assay with tol6 variants. Equal amounts of bead-bound different TOL6 constructs or beads incubated with only bacterial lysate as control (TOL6:6xHis, or tol6:6xHis, 75 kDa, open arrowhead, bottom panel, probed with anti His-antibody, α-His) were incubated with equal amounts K63-linked di-ubiquitin (17 kDa, arrowhead, middle panel). Precipitated proteins were probed with α-ubq (arrowhead, top panel). While K63-linked di-ubiquitin clearly co-precipitated with TOL6:6xHis, tol6^{mVHS}:6xHis co-precipitated less and tol6^{mGAT}:6xHis even less. Very little co-precipitation could be detected with tol6^{mTOTAL}:6xHis and none at all with the beads incubated with bacterial lysate alone (arrowhead, top panel). Normalized signal intensities are indicated below blots, and the strongest signal in each experiment was arbitrarily set to 1.

ubiquitin, or GST alone as negative control (Figure 3C, bottom panel), were incubated with equal amounts of the different bacterially expressed, purified His-tagged TOL6 proteins (Figure 3C, middle panel). The analyzed precipitate showed that TOL6:6xHis clearly co-precipitates with GST:ubiquitin and not with GST alone, and that ubiquitin binding was only slightly weaker than with tol6^{mVHS}:6xHis (Figure 3C, top panel). A striking difference was seen with both tol6^{mGAT}:6xHis and tol6 ^{mTOTAL}:6xHis, where the binding to the ubiquitin beads is distinctly reduced (Figure 3C, top panel). We verified these results in linkage-specific ubiquitin-binding assays, demonstrating a complete loss of binding of beads-coupled GST:N-term.tol6^{mTOTAL} when precipitating K63-linked di-ubiquitin (Supplemental Figure 4E). To validate that these differences are not affected by the ability of the GST tag to dimerize (Sims et al., 2009), we performed the same assays, employing His-tagged variants of TOL6 (Figure 3D), coupled to Ni–Sepharose beads and incubating them with equal amounts of K63-linked di-ubiquitin (Figure 3D). The highest amount of K63-linked di-ubiquitin was precipitated with non-mutated TOL6, while the VHS-mutated version showed slightly weaker ability to pull down the di-ubiquitin (Figure 3D). This difference was substantially more pronounced for tol6^{mGAT}:6xHis and tol6^{mTOTAL}:6xHis (Figure 3D). In summary, we were able to show that mutations of conserved amino acids in both UBD domains of TOL6 greatly reduced its ability to bind to GST-tagged mono-ubiquitin and K63-linked di-ubiquitin *in vitro*, demonstrating involvement of the N-terminal UBDs of TOL6 in the binding of ubiquitin *in vitro*. Taken together,the above results demonstrate that *TOL* function is linked to the recognition of ubiquitinated proteins, where TOL2 and TOL6 show a strong preference for K63-linked ubiquitin chains via their N-terminal UBDs. This type of TOL–substrate interaction could function as prerequisite for further cargo sorting via the ESCRT machinery, potentially via the ESCRT-I subunit VPS23A (Figure 2).

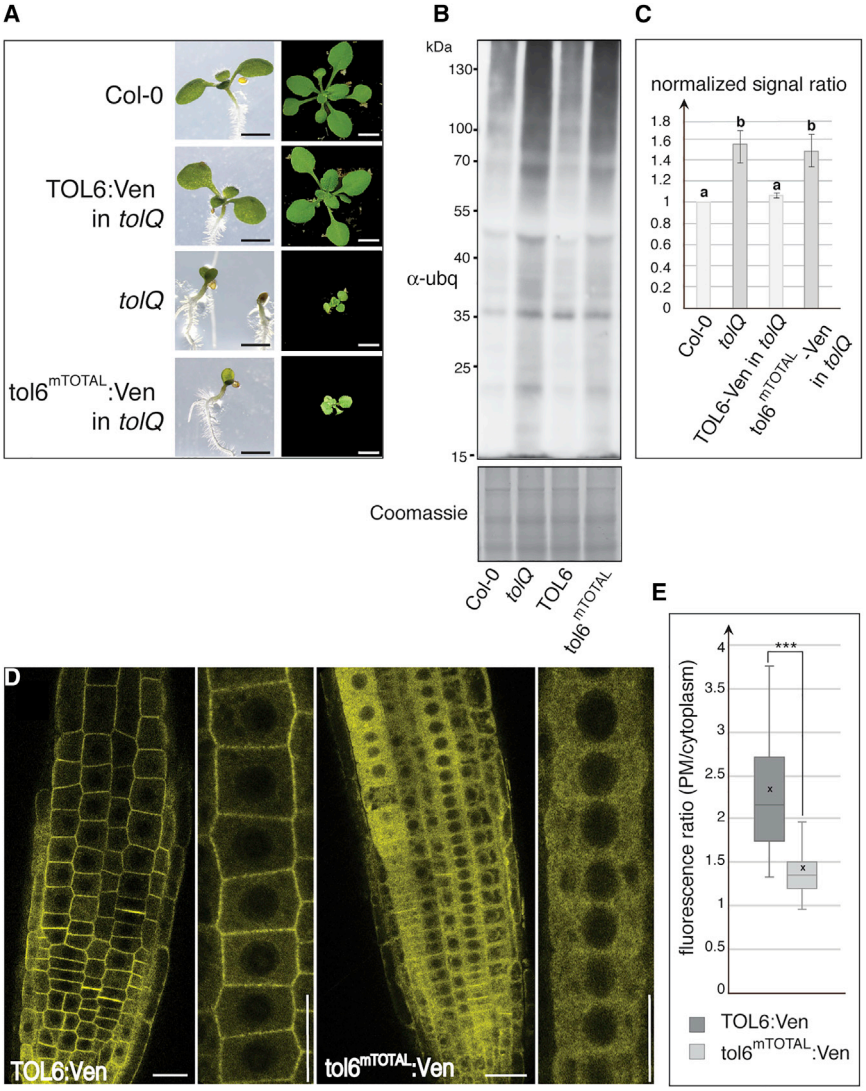

Figure 4. The UBD-Mutated Version of TOL6 Is Non-functional.

(A) Phenotypes of Col-0, TOL6:Ven in *tolQ*, *tolQ*, and tol6^{mTOTAL}:Ven in *tolQ* plants. Seven-day-old seedlings (left row; scale bars: 2 mm) and 17-day-old rosettes (right row; scale bars, 5 mm).

(B) Total leaf protein extracts of Col-0 (lane 1), *tolQ* (lane 2), *TOL6p*::*TOL6*:*Ven in tolQ* (lane 3), and *TOL6p*::*tol6*^{mTOTAL}:*Ven* in *tolQ* (lane 4) were subjected to SDS–PAGE and immunoblotting and probed with α-ubq (top panel) or SDS–PAGE and Coomassie staining as loading control (bottom panel). Note the accumulation of ubiquitin conjugates in *tolQ*, which could be reverted by expression of TOL6:Ven in the same background, but not by tol6^{mTOTAL}:Ven.

(C) Statistical evaluation of differences in the signal intensities of the ubiquitination patterns in Col-0, *tolQ*, *TOL6p*::*TOL6*:*Ven in tolQ*, or *TOL6p*::*tol6mTOTAL*:*Ven* in *tolQ* plant lines. Average gray values in areas of identical size and shape of total lanes were determined and normalized to the average gray values of the entire lane of the corresponding Coomassie brilliant blue staining signal. The resulting normalized signal ratios between Col-0 and the other plant lines are presented as means ± SD (n = 3 biological replicates). The different letters above each bar indicate statistically significant differences as determined by one-way ANOVA with post hoc Tukey HSD test ($p \leq 0.01$).

(D) Signal distribution in root epidermal meristem cells of 6-day-old plants expressing *TOL6p*::*TOL6*:*Ven* (left two panels) or *TOL6p*::*tol6*^{mTOTAL}:*Ven* (right two panels) in *tol6-1* background. Scale bars, 25 μm.

(E) Relative signal intensities (signal at PM normalized to signal intensities in cytoplasm) of TOL6:Ven and tol6^{mTOTAL}:Ven in *tol6-1* root meristem cells (125–130 root epidermal cells from three independent biological repeats were tested for each dataset and analyzed by one-way ANOVA with post hoc Tukey HSD test; $^{***}p \leq 0.001$).

A Ubiquitin-Binding-Deficient Version of TOL6 Shows Altered Subcellular Localization and Is Not Functional *In Planta*

To decipher the effects of the mutated UBDs on the function of TOL6 *in vivo*, we generated reporter plant lines expressing either wild-type *TOL6* or the ubiquitin-binding-deficient *tol6*^{mTOTAL} fused to Venus under control of the *TOL6* promoter and transformed them into *tolQ*. TOL6:Ven fully rescued the *tolQ* phenotype, resembling Columbia-0 (Col-0) wild-type plants at all stages of development (Figure 4A; Supplemental Figure 5A and 5B), as we previously reported for the same construct with a different tag (Korbei et al., 2013). Contrarily, ubiquitin-binding-deficient *tol6*^{mTOTAL} completely failed to complement the *tolQ* phenotype (Figure 4A; Supplemental Figure 5A and 5B), although both lines expressed the transgenes at similar levels (Supplemental Figure 5C, left panels), indicating that tol6^{mTOTAL}:Ven differs in its functionality from the wild-type protein (Figure 4A). Tol6^{mTOTAL}:Ven also failed to rescue defects in the degradation of ubiquitinated proteins that is characteristic for *tolQ* (Figure 4B). While total protein extracts from leaves from plants expressing TOL6:Ven in *tolQ* accumulated ubiquitin conjugates at levels comparable with those in wild-type plants (Figure 4B and 4C), *tolQ TOL6p*::*tol6*^{mTOTAL}:*Ven* extracts showed higher levels of ubiquitin conjugates (Figure 4B and 4C), similar to the levels found in extracts from *tolQ* plants (Figure 4B and 4C).

We further asked whether the *tol6*^{mTOTAL} mutant would also have an effect on the spatial control of *TOL6*. We therefore transformed the aforementioned *TOL6* reporter constructs into the *tol6-1* background. Both tol6^{mTOTAL}:Ven and TOL6:Ven are expressed at similar levels and give proteins of the expected size when analyzing total plant extracts (Supplemental Figure 5C). TOL6:Ven localized to the PM and in early endosomes (Figure 4D), indicated by signal overlaps with the endocytosed styryl dye FM4-64 after short-pulsed staining (Supplemental Figure 5D), similar to TOL6:mCherry (Korbei et al., 2013). Mutated tol6^{mTOTAL}:Ven, however, no longer localized at the PM but was predominantly cytoplasmic (Figure 4D and

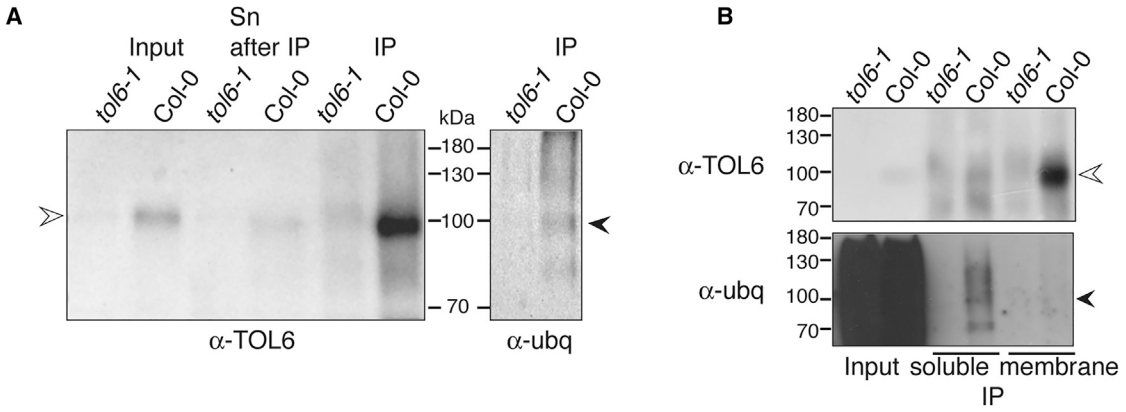

Figure 5. TOL6 Is Ubiquitinated *In Planta*.

(A) Immunoprecipitations (IPs) were performed from 7-day-old *tol6-1* and Col-0 root extracts with protein A magnetic beads coupled to an affinity-purified TOL6 antibody (α-TOL6) and the precipitate subjected to immunoblotting and probed with α-TOL6 (open arrowhead, left panel) or with a ubiquitin-specific antibody (α-ubq, arrowhead, right panel) to test for specific ubiquitination. Sn, supernatant.

(B) TOL6 IPs out of the membrane and soluble fractions performed from *tol6-1* and Col-0 7-day-old root extracts with beads coupled to α-TOL6 as described by Waidmann et al. (2018). The precipitate was subjected to immunoblotting and probed with α-TOL6 (top panel). The left lanes show the input amount while right lanes represent total eluted protein from the beads of the membrane or the soluble fraction. Endogenous TOL6 is clearly visible in the Col-0 input, as well as after IP in both Col-0 membrane and soluble fractions (open arrowhead), while it is missing in *tol6-1* extracts. The IP probed with α-ubq antibody (bottom panel) showed a band at the same height as TOL6 (arrowhead) only in the soluble fraction of the Col-0 samples, demonstrating that the soluble fraction of TOL6 is ubiquitinated. All IPs were performed in RIPA buffer.

Supplemental Figure 5D). This difference in localization is statistically highly significant (Figure 4E), providing strong evidence for an involvement of UBDs in localization control of TOL6.

We show that a ubiquitin-binding-deficient *tol6* allele not only is non-functional in the degradation pathway of ubiquitinated cargo but also exhibits aberrant intracellular localization. Such adjustments in subcellular distribution might reflect regulatory aspects of TOL function in cargo sorting, potentially hinting at a mechanism by which TOL6–ubiquitin interaction impacts on intracellular localization.

TOL6 Is Ubiquitinated, Specifically in Its Soluble Fraction

Almost as soon as UBDs were discovered, it was established that many ubiquitin receptors are themselves ubiquitinated, which does not lead to their degradation but rather serves as a regulatory signal (Hicke et al., 2005; Hoeller and Dikic, 2010). As recent plant ubiquitome studies have shown that several endocytic adaptors, including the TOLs, are ubiquitinated (Svozil et al., 2014; Walton et al., 2016), we decided to investigate the ubiquitination of TOLs *in vivo* and to assess the potential effect of this ubiquitination. We therefore performed immunoprecipitation (IP) of the endogenous TOL6, using beads crosslinked with an affinity-purified anti-TOL6 antibody (Supplemental Figure 6), from wild-type plants and *tol6-1* null plants. These experiments revealed a significant portion of the precipitated TOL6 to be ubiquitinated when probed with P4D1, a general anti-ubiquitin antibody (α-ubq), whereas no corresponding signals could be detected in *tol6-1* controls (Figure 5A).

We then initiated experiments aimed at testing for functional implications of TOL6 ubiquitination. We therefore probed TOL6 immunoprecipitates from solubilized wild-type (Col-0) membrane extracts with a non-discriminating ubiquitin antibody and compared them with TOL6 immunoprecipitated out of equal amounts of the soluble protein fraction (Figure 5B), using a well-established protocol for the separation of the soluble and membrane fractions (Leitner and Luschnig, 2014). We observed a continuous signal, starting approximately at the molecular weight of TOL6, in the soluble fraction of Col-0. No signals were observed in IPs either from Col-0 membrane fractions or out of IPs performed with soluble and membrane fractions from *tol6-1* plant lysates, indicating ubiquitination of preferentially the soluble portion of the endogenous TOL6 (Figure 5B). These results demonstrate ubiquitination of endogenous TOL6, predominantly in the soluble protein fraction, indicative of scenarios in which TOL6 ubiquitination could have a regulatory function, by antagonizing TOL6 localization at the PM.

A Constitutively Ubiquitinated TOL6 Shows Altered Subcellular Localization and Is Not Fully Functional

To further dissect functional implications of TOL6 ubiquitination, we generated a TOL6 construct fused at its C terminus to a ubiquitin where, to prevent processing by ubiquitin proteases, the C-terminal two glycines were replaced by alanines (Hershko and Ciechanover, 1998). Such fusions have been shown to mimic constitutive ubiquitination (Hoeller et al., 2006; Leitner et al., 2012). As many helical UBDs are known to interact with a single region on ubiquitin, the hydrophobic patch around I44 (Husnjak and Dikic, 2012), we generated a construct in which we replaced the isoleucine in ubiquitin at position 44 by an alanine (I44A), whereby binding to UBDs should be greatly reduced (Hicke et al., 2005), rendering the ubiquitin tag non-functional (Figure 6A). This serves as a control to exclude effects due to misfolding or steric hindrances imposed by the fusion of ubiquitin to TOL6. We further added a C-terminal Venus tag and expressed the entire cassette under control of

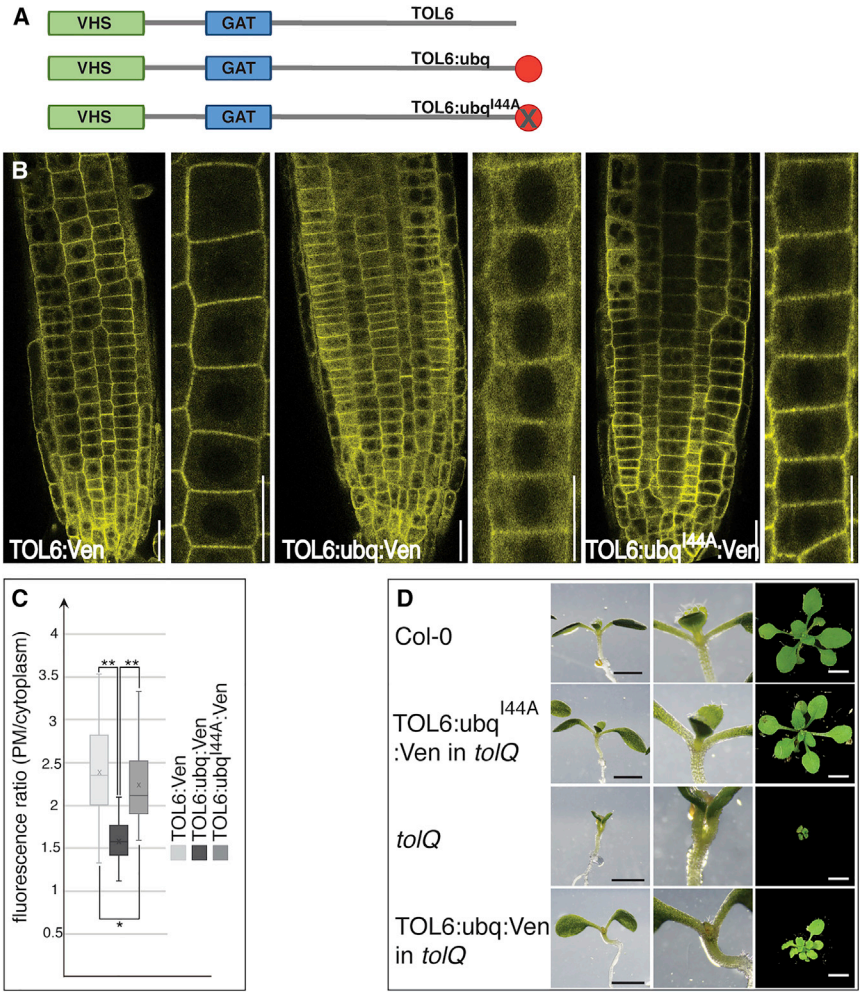

Figure 6. A Constitutively Ubiquitinated Version of TOL6 Is Non-functional.

(A) Schematic representation of ubiquitin chimeras used. Red circle represents ubiquitin and red circle with X the mutated ubiquitin^{I44A}.

(B) Signal distribution in root epidermal meristem cells of 6-day-old plants expressing *TOL6p*::*TOL6*:*Ven* (left two panels), *TOL6p*::*TOL6*:*ubq*:*Ven* (middle two panels), or *TOL6p*::*TOL6*:*ubq^{I44A}*:*Ven* (right two panels) in *tol6-1* background. Scale bars, 25 μm.

(C) Relative signal intensities (signal at PM normalized to signal intensities in cytoplasm) of TOL6:Ven, TOL6:ubq:Ven, or TOL6:ubq^{I44A}:Ven in *tol6-1* root meristem cells (71–97 root epidermal cells from three independent biological repeats were tested for each dataset and analyzed by one-way ANOVA with post hoc Tukey HSD test; $^{**}p \leq 0.01$, $^{*}p \leq 0.05$).

(D) Phenotypes of Col-0, *TOL6p*::*TOL6ubq*:*Ven* in *tolQ*, *tolQ*, or *TOL6p*::*TOL6*:*ubq^{I44A}*:*Ven* in *tolQ*. Seven-day-old seedlings (left row; scale bars, 2 mm), with a close up of shoot apical meristem (middle row) and 17-day-old rosettes (right row; scale bars, 5 mm).

the *TOL6* promoter, and introduced *TOL6*:*ubq*:*Ven* and *TOL6*:*ubq^{I44A}*:*Ven* into the *tol6-1* and the *tolQ* background. Although ubiquitination is often a signal for degradation (Clague and Urbe, 2010; Dubeaux and Vert, 2017), no striking differences could be observed in TOL6:ubq:Ven steady-state protein levels when compared with TOL6:ubq^{I44A}:Ven or TOL6:Ven in *tol6-1* backgrounds, even when treated with different proteasome inhibitors (Supplemental Figure 7B). Thus, the ubiquitin tag does not destabilize the protein.

Remarkably, TOL6:ubq:Ven showed a strong tendency to locate to the cytoplasm while the mutant TOL6:ubq^{I44A}:Ven fusion protein restored reporter protein signals at the PM, exhibiting a signal distribution similar to wild-type TOL6:Ven (Figure 6B and Supplemental Figure 7C). These differences in localization support scenarios in which a functional ubiquitin tag triggers relocation of TOL6 from the PM.

Differences in intracellular distribution of TOL6:ubq:Ven, when compared with TOL6:ubq^{I44A}:Ven, are suggestive of a regulatory role of TOL6 ubiquitination. This hypothesis was addressed further by testing the functionality of the TOL6:ubq proteins based on their ability to rescue *tolQ* growth deficiencies. While the TOL6:ubq chimera failed to fully rescue the pronounced *tolQ* phenotype, the functionality of the TOL6:ubq^{I44A}:Ven construct was not compromised (Figure 6D). The I44A mutation in the ubiquitin chimera completely restored the ability of the construct to function like wild-type TOL6:Ven, presumably by rendering the ubiquitin tag non-functional (Figure 6D). Seven-day-old seedlings (Figure 6D and Supplemental Figure 7D) and 17-day-old plants (Figure 6D) expressing the mutated ubiquitin chimera were similar in size and development to Col-0 wild-type controls and to *tolQ* expressing fully rescuing TOL6:Ven (Figures 4A and 6D). In contrast, 7-day-old seedlings from *tolQ* expressing TOL6:ubq:Ven exhibited a variety of alterations in their developmental phenotypes, from delayed growth to aberrant formation of the first true leaves as well as alterations in rosette formation and size (Figure 6D). Furthermore, root length was significantly different from those of Col-0, *tolQ TOL6p*::*TOL6*:*ubq^{I44A}*:*Ven*, and *tolQ* (Supplemental Figure 7D and 7E). The adult plants partially recovered and did not show the typical *tolQ* dwarfed phenotype, although they were smaller and produced fewer seeds than complementary *tolQ TOL6p*::*TOL6*:*Ven* controls (Supplemental Figure 7F). To assess whether these defects could be brought about by a difference in TOL ESCRT-I interaction, we performed *in vitro* binding assays combining VPS23A and the modified TOL6 versions, but no obvious differences in binding could be detected (Supplemental Figure 8). Thus, the inability of TOL6:ubq (as well as tol6^{mTOTAL}) to complement the *tolQ* phenotype is likely not caused by a loss of interaction with VPS23A and thus, potentially, with the ESCRT machinery.

When analyzing leaf total protein extracts from *tolQ TOL6p*::*TOL6*:*ubq*:*Ven* plants, we observed differences in the degradation of ubiquitinated cargoes (Figure 7A and 7B). While global ubiquitination appeared unaltered in *tolQ*

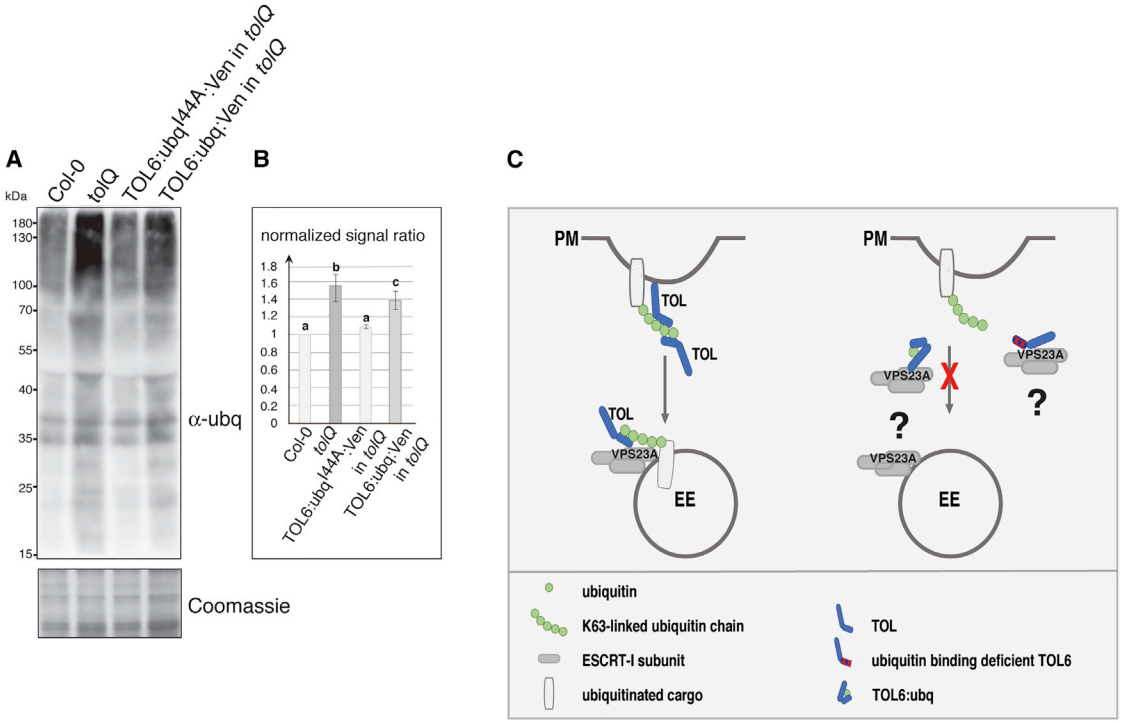

Figure 7. TOL6 Function in the Degradation of K63-Ubiquitinated PM Proteins.

(A) Total leaf protein extracts of Col-0 (lane 1), *tolQ* (lane 2), *TOL6p*::*TOL6*:*ubq*^{I44A}:*Ven* in *tolQ* (lane 3), or *TOL6p*::*TOL6*:*ubq*:*Ven in tolQ* (lane 4) were subjected to western blotting and probed with a ubiquitin antibody (α-ubq; top panel). Note the accumulation of ubiquitin conjugates in *tolQ*, which could be reverted by expression of TOL6:ubq^{I44A}:Ven in the same background, but not by TOL6:ubq:Ven. Coomassie staining (bottom panel) was used as a loading control.

(B) Statistical evaluation of differences in the signal intensities of the ubiquitination patterns in Col-0, *tolQ*, and *TOL6p*::*TOL6*:*ubq*:*Ven* or *TOL6p*::*TOL6*:*ubq*^{I44A}:*Ven tolQ*. Average gray values in areas of identical size and shape of total lanes were determined and normalized to the average gray values of the entire lane of the corresponding Coomassie brilliant blue staining signal. The resulting normalized signal ratios between Col-0 and the other plant lines are presented as means ± SD (n = 3 biological replicates). The different letters above each bar indicate statistically significant differences as determined by one-way ANOVA with post hoc Tukey HSD test ($p \leq 0.01$).

(C) A proposed model for the potential role of TOL2 and TOL6 in the degradation pathway of ubiquitinated PM proteins. TOL proteins recognize (preferentially K63-linked) ubiquitinated PM proteins destined for degradation at the PM and help guide them to the ESCRT-I machinery at the TGN/EEs (left side). If the TOL function is inhibited, either by ubiquitination of the TOL protein, or because the UBD is non-functional, PM protein degradation does not function appropriately (right side). TOL6:ubq represents the reporter protein,? represents the position of the ESCRT-I complex in the *TOL6p*::*tol6*^{mTOTAL}:*Ven* in *tolQ*, *TOL6p*::*TOL6*:*ubq*:*Ven* in *tolQ* or *tolQ* plant lines, which is currently not established.

TOL6p::*TOL6*:*ubq*^{I44A}:*Ven* total plant lysates (Figure 7A and 7B), *tolQ TOL6p*::*TOL6*:*ubq*:*Ven* extracts showed an elevated global ubiquitination level (Figure 7A and 7B), albeit not as severe as in *tolQ* (Figure 7A and 7B), demonstrating that the inability of TOL6:ubq:Ven to fully rescue *tolQ* defects coincides with deficiencies in the degradation of ubiquitinated proteins. Thus, a constitutively ubiquitinated version of TOL6 exhibits differences in its subcellular localization and is not fully functional in turnover of ubiquitinated cargo, while a version with a non-functional ubiquitin tag behaves like the wild-type version of TOL6, consistent with a function for reversible ubiquitination in the regulation of TOLs.

DISCUSSION

Plants have developed a myriad of different pathways in their prevailing need to be able to respond quickly and accurately to environmental stimuli. Receptors and transporters in the PM are essential for this fast response; thus, their abundance has to be strictly controlled. The hetero- and multimeric ESCRTs machinery is responsible for mediating the degradation of endocytosed ubiquitinated PM proteins in eukaryotes (Paez Valencia et al., 2016; Gao et al., 2017; Isono and Kalinowska, 2017). Modification by K63-linked ubiquitin chains is the second most abundant form of protein ubiquitination (Kim et al., 2013; Erpapazoglou et al., 2014; Tomanov et al., 2014) and is essential for the proper sorting of endocytosed PM proteins into ILV of MVBs before reaching the vacuole for subsequent degradation (Dubeaux and Vert, 2017; Isono and Kalinowska, 2017; Romero-Barrios and Vert, 2018). Several proteins have been shown to be K63-linked poly-ubiquitinated *in planta* (Kasai et al., 2011; Leitner et al., 2012; Martins et al., 2015), and over 100 plant proteins conjugated with K63-linked chains were identified recently (Johnson and Vert, 2016). Endocytic vesicles co-localize with K63-linked cargo (Johnson and Vert, 2016), and molecular mechanisms driving K63-linked poly-ubiquitin-dependent endocytosis are essentially conserved. Nevertheless, plants have developed numerous plant-specific factors and special properties, especially in the early steps of endosomal trafficking of PM protein destined for degradation

(Dubeaux and Vert, 2017; Gao et al., 2017). Thus, many unique proteins have been identified to be involved in the regulation of endosomal trafficking, and some ESCRT subunits have undergone drastic gene expansions (Sauer and Friml, 2014; Gao et al., 2017; Isono and Kalinowska, 2017; Otegui, 2018).

In this study we have established TOL2 and TOL6 and thus, potentially, TOLs in general as functional substitutes of the elusive ESCRT-0 in plants. Our current working model implies that TOL2 and TOL6 bind to K63-linked ubiquitin chains, thereby controlling degradation of ubiquitinated proteins. This seemingly involves interaction with the ESCRT machinery, as indicated by TOL2 and TOL6 interaction with ESCRT-I subunit VPS23A. Consistent with such a role, we found that interference with substrate recognition by mutagenizing TOL6 UBDs preferentially interferes with binding to K63-linked ubiquitin. This coincides with TOL6 mislocalization and an overall loss in functionality, which was also observed for constitutively ubiquitinated TOL6:ubq, although to a lesser degree (Figure 7C).

We focused on the PM-localized and early endosome-localized TOL6 as well as the cytoplasmic TOL2 as representatives for the TOL protein family. The cytoplasmic TOL5, which is also found in the endocytic membrane fractions (Korbei et al., 2013), has been described to function at MVBs, where it co-localizes with BOR1 on its route to the vacuole under high-boron conditions (Yoshinari et al., 2018). Thus, TOL proteins might also participate in recognition and sequestration of ubiquitinated cargoes at the limiting membrane of MVBs. Consistent with diverging but still overlapping functions of TOLs, we found that only higher-order *tol* knockouts markedly inhibit not only the downregulation of specific PM-localized ubiquitinated proteins (Korbei et al., 2013; Yoshinari et al., 2018) but also ubiquitin-conjugated cargoes in general (this study). Both TOL2 and TOL6 interact with the ESCRT machinery via VPS23A and show a pronounced substrate preference to K63-linked ubiquitin via VHS and GAT domains, as mutation of these for TOL6 resulted in complete loss of ubiquitin binding. The tandemly arranged UBDs, which have been shown to permit the recognition of poly-ubiquitin chains with increased affinity over free ubiquitin (Sims and Cohen, 2009; Lange et al., 2012), are also present in all other TOLs and can regulate kinetics and fidelity of the endocytosed ubiquitinated cargoes destined for degradation.

One could envision that TOLs function in a network in the plant endomembrane system, where they hand over the ubiquitinated cargo in its path toward the vacuole. Apart from conserved UBDs at the N terminus, TOLs differ substantially in their C-terminal domains (Korbei et al., 2013). Ubiquitin receptors usually have additional modular structures, which might be relevant for potential membrane or clathrin binding or protein–protein interactions, and these multivalent interactions might help regulate localization, oligomeric state, and additional binding partners. It will therefore be important to learn about how different C-terminal domains of different TOLs contribute to their distinct localization and, therefore, function.

Specificity in cargo recognition could be enhanced by oligomerization of ubiquitin receptors functioning as a multivalent ubiquitin-binding complex, as was shown for the ESCRT-0 complex (Ren and Hurley, 2010). This clustering of interactions, with low affinities yet high specificity, creates a network that is fluid and can undergo rapid assembly and disassembly. Therefore, destabilization of the network to, for example, disengage from the ubiquitinated cargo, could be accomplished by a simple alteration of individual domains of the proteins in the network. This could explain the altered localization and complete loss of functionality that we observed for the UBD-mutated *tol6* allele, which was not caused by disengagement from the ESCRT machinery. Alternatively, as cargo ubiquitination promotes the association of ESCRTs with membranes (MacDonald et al., 2012), TOLs unable to bind ubiquitinated cargo could simply not be associated with membranes any longer. Thus, there is much to be discovered when it comes to the spatial or temporal targeting of the ubiquitin network.

Many ubiquitin receptors are themselves ubiquitinated, which does not lead to their degradation but rather serves as a regulatory signal (Hicke et al., 2005; Hoeller and Dikic, 2010). Ubiquitination of UBD-containing proteins imposes an autoinhibitory conformation, rendering them unable to bind in *trans* to ubiquitinated targets (Hoeller and Dikic, 2010), serving as an intrinsic switch-off mechanism (Fallon et al., 2006; Hoeller et al., 2006). Functional significance for this type of regulation has been provided by studies employing constitutively ubiquitinated versions of the endocytic UBD-containing proteins (Hoeller et al., 2006). Furthermore, in mammalian systems the non-selective deubiquitinating enzyme USP8 and the stringent K63-linked ubiquitin chain-selective deubiquitinating enzyme AMSH compete for binding to ESCRT-0 subunits (Clague et al., 2019), in order to deubiquitinate and stabilize them (Row et al., 2006) or to modulate their activity by altering their ubiquitination status (Sierra et al., 2010). This underlines that the ubiquitination status of ubiquitin receptors acts as an important regulatory interface.

We have shown that a fraction of endogenous TOL6 is ubiquitinated *in planta*, a modification seemingly not involved in control of the protein half-life but rather affecting the regulation of cargo sorting, via spatiotemporal control of subcellular TOL distribution. This is indicated further by the fact that preferentially TOL6 in the soluble fraction exhibits pronounced ubiquitination, and a TOL6–ubiquitin fusion mimicking ubiquitination not only altered protein functionality but also affected its subcellular localization, with a shift from the PM into the cytosol. Reversible ubiquitination of the TOLs could thus serve as a switch from a PM-localized, sorting competent TOL6 pool that is not ubiquitinated to ubiquitinated TOL6 localized in the cytoplasm that is no longer sorting competent. Some of the TOLs might thus be subject to dynamic spatiotemporal regulation of their abundance at or close to the PM, which could be a means to modulate the degradation of PM proteins. This might also explain the spatiotemporal variations of TOL6 localization observed in gravistimulated root meristems, potentially contributing to differential turnover of the PIN2 cargo protein (Korbei et al., 2013). If true, then such spatiotemporal regulation of the nine TOLs might fine-tune the function of TOLs as ubiquitin adaptors in diverse trafficking processes. The occurrence of such mechanisms would support the notion of a dual role for ubiquitin in endocytic pathways, acting as sorting tag on trafficking cargoes as well as a regulatory signal on UBD-containing proteins.

Disrupting either the ubiquitination of, or ubiquitin binding by, TOL6 affected the localization and function of the protein. All

things considered, such ubiquitination and ubiquitin binding may help hold components of the early endosomal machinery together (Dores et al., 2010; Weinberg and Drubin, 2014). This situation provides many targets for regulation because the disruption of any such interactions could lead to network reorganization. The combined usage of several UBD-containing proteins involved in selective recognition of cargo proteins as well as their potential post-translational modifications illustrates how ubiquitin receptors can control cellular functions. Ubiquitination of the TOLs could thus contribute to the control of PM-localized cargo steady-state levels by influencing the intersection between protein recycling and downregulation.

METHODS

Cloning Procedures

All primers used for cloning are listed in Supplemental Table 1. All clones were confirmed by sequencing.

TOL5p::*TOL5*:*Ven*, *TOL6p*::*TOL6*:*Ven*, *TOL6p*::*TOL6*:*ubq*:*Ven*, and *TOL6p*::*TOL6*:*ubq*^{I44A}:*Ven* were obtained by replacing mCherry in *TOL5p*::*TOL5*:*mCherry* or *TOL6p*::*TOL6*:*mCherry* (Korbei et al., 2013) with the Venus tag (Ven), which were PCR amplified with the primer pair NotImcherryu/NotImcherryd from *PIN2p*::*PIN2*:*VEN*, or *ubq*:*Ven* and *ubq*^{I44A}:*Ven*, which were PCR amplified with the primer pair with mcherryNotIdown/NotIUbqVenusf from *PIN2p*::*PIN2*:*ubq*:*VEN* or *PIN2p*::*PIN2*:*ubq*^{I44A}:*VEN*, respectively (Leitner et al., 2012).

TOL2p::*TOL2*:*Ven*, *TOL3p*::*TOL3*:*Ven*, and *TOL9p*::*TOL9*:*Ven*, approximately 1.5–2 kb upstream of the *TOL2*, *TOL3*, and *TOL9* ORFs, were amplified with primers pTOL2f/pTOL2r (for TOL2p), pTOL3f/pTOL3r (for TOL3p), and pTOL9f/pTOL9r (for TOL9p) and ligated via XmaI/XbaI for TOL2p, XbaI for TOL3p, and KpnI/BamHI for TOL9p into a derivative of pPZP221 containing a pApA terminator as described in Leitner et al. (2012). cDNAs of TOL2 (1152 bp), TOL3 (1545 bp), and TOL9 (2031 bp) were amplified by PCR with primer pairs TOL2-SalIu/TOL2-NotISalIr (TOL2), TOL3-SalIu/TOL3-NotISalIr (TOL3), and TOL9-SalIu/TOL9-NotISalIr (TOL9) and cloned into a standard cloning vector (pTZ57R/T). A PCR-amplified Ven (see above) was inserted into the NotI site and the entire cassette was cloned into the SalI site of the pPZP221 pApA already containing the respective promoter construct.

For the *TOL6p*::*tol6*^{mTOTAL}:*Ven* plant expression, a Venus tag amplified as described above was cloned into *tol6*^{mTOTAL}in pTZ57R/T (see below) via NotI, then *tol6*^{mTOTAL}:*Ven* was amplified from the pTZ57R/T vector with TOL6-SalIu/TOL6-NotISalIr and inserted into the SalI site of a derivative of pPZP221 containing the terminator pApA and already containing the TOL6 promoter upstream as described by Korbei et al. (2013).

TOL6 cDNA in pTZ57R/T (Korbei et al., 2013) was amplified with oligos TOL6W25Af/TOL6W25Ar and subsequently with oligos TOL6N73Af/TOL6N73Ar to mutate W25A and N73A, to obtain *tol6*^{mVHS}. *TOL6* cDNA in pTZ57R/T (Korbei et al., 2013) was amplified with oligos TOL6AAA1f/TOL6AAA1f to replace DLL by AAA at position 246–248 and subsequently with oligos TOL6AAA2f/TOL6 AAA2r to replace DML by AAA at position 250–252, resulting in *tol6*^{mGAT}. The total mutant TOL6, including both VHS and GAT mutations, was obtained by using EcoRI as restriction enzyme to insert the first 424 bp from *tol6*^{mVHS} in pTZ57R/T into *tol6*^{mGAT}, resulting in *tol6*^{mTOTAL}.

For bacterial expression, tol6^{mVHS}, tol6^{mGAT}, and tol6^{mTOTAL} were amplified from their corresponding constructs in pTZ57R/T vectors using primer pair TOL6-SalIu/TOL6-SalId followed by ligation into the SalI site of pET24a (Novagen). For TOL6:ubq and TOL6:ubq^{I44A}, ubq or ubq^{I44A} were amplified with primers NotIUbqpET24af/UbqNotIr from *PIN2p*::*PIN2*:*ubq*:*VEN* or *PIN2p*::*PIN2*:*ubq*^{I44A}:*VEN*, respectively (Leitner et al., 2012) and ligated into NotI-digested TOL6 in pET24a (Korbei et al., 2013).

For the N-terminal, TOL6, or N-term.tol6^{mTOTAL} construct, the respective constructs in the pET24a vectors were amplified with the oligos TOL6-SalIu/TOL6-VHSGAT-SalIr and cloned via SalI into pGEX4T-3 to obtain the GST-tagged versions.

Full-length VPS23A and N-terminal VPS23A coding DNA were amplified by PCR with primer pairs BamHIELCf/ELCSalIr or BamHIELCf/ELC(UEV-C) SalIr and cloned between the BamHI and SalI site of pGEX4T-1.

C-terminal VPS23A (GST:VPS23A(ΔUEV) [Nagel et al., 2017]), TOL6:6xHis, TOL2::6xHis, and GST:ubq (Korbei et al., 2013) were described previously.

Plant Transformation and Analysis of Transgenic Lines

Flowering *Arabidopsis* plants were transformed with *Agrobacterium tumefaciens* (with the appropriate constructs as described in main text) into *tol2-1*, *tol3-1*, *tol5-1*, *tol6-1*, *tol9-1*, or *tol2-1*/*tol2-1*, *TOL3*/*tol3-1*, *tol5-1*/*tol5-1*, *tol6-1*/*tol6-1*, *tol9-1*/*tol9-1* plants using the floral dip method (Clough and Bent, 1998). Resulting T2 lines were confirmed for single-transgene insertion sites and propagated for further analysis. At least three independent transformants were characterized for each line. Homozygous plants were confirmed by PCR genotyping for the mutant alleles.

Genotyping was performed based on PCR with the primer combinations described by Korbei et al. (2013) for all T-DNA insertion lines and primer pair Venus-qPCRF1/pApAu (see Supplemental Table 1) for tagged reporter constructs in the plant expression vector.

SDS–PAGE, Coomassie brilliant blue staining, and immunoblotting were performed according to the standard protocols, with the addition that for ubiquitin blots we boiled the nitrocellulose membranes before blocking, according to Leitner and Luschnig (2014).

Antibodies

Primary Antibodies

Mouse-anti-ubq antibody (P4D1, Santa Cruz Biotechnology; sc-8017); His·Tag monoclonal antibody (Novagen/EMD Millipore; 70796-4); mouse-anti-GFP antibody (Roche 11814460001); GST Tag monoclonal antibody (8-326; Thermo Fischer Scientific; MA4-004); monoclonal anti-α-tubulin antibody (Sigma; T6074); HA-Tag (C29F4) rabbit monoclonal antibody (Sigma-Aldrich; #3724); anti-VP16 antibody (Abcam; ab4808).

A TOL6-specific polyclonal antibody was raised in rabbits against full-length TOL6 His-tagged protein (TOL6:6xHis) and the rabbit serum was affinity purified before use, using the blotted antigen.

Secondary Antibodies

Goat anti-mouse immunoglobulin G (IgG) (horseradish peroxidase [HRP]-linked antibody; Jackson ImmunoResearch; 115-035-164); anti-rabbit IgG (HRP-linked antibody; Cell Signaling Technologies; 7074).

Protein Extraction

Small-scale total protein extraction for western blotting was performed from 20 mg of 6-day-old seedlings. Grinding of the frozen plant material was performed with a Retsch mill and extracted in 150 μl of buffer (65 mM Tris [pH 6.8], 5% β-mercaptoethanol, 2% SDS, 10% glycerin, 0.25% bromophenol blue, 8 M urea), heated at 65°C for 5 min, and spun down before loading.

Ubiquitination Assays

Global ubiquitination assays were performed as described by Kalinowska and Isono (2014), but grinding of the frozen plant material (either 100 mg of 6-day-old seedlings or 100 mg of adult leaves [rosette and cauline

leaves]) was performed with a Retsch mill and metal balls, and 20 mM NEM (*N*-ethylmaleimide; Sigma) was added freshly to the protein extraction buffer. For assessment of differences in the signal intensities of the ubiquitination patterns, average gray values in areas of identical size and shape using ImageJ/Fiji software were determined in total lanes normalized either to the average gray values of the corresponding tubulin signals or the Coomassie brilliant blue staining signal of the entire lane. The average of three different exposure times for each western blot for each individual biological repeat was used. At least three biological repeats per performed. Resulting signal ratios were depicted as box plots, and their statistical significance was calculated using one-way ANOVA with a post hoc Tukey HSD (honestly significant difference) test.

Microscopy

CLSM images were generated using a Leica SP5 (Leica Microsystems, Wetzlar, Germany) microscope. For imaging, we used the following excitation conditions: 514 nm (Venus); 561 nm (RFP and FM4-64). For assessment of the reporter signal distribution of the different Ven-tagged *TOL* alleles as well as *TOL6* variant alleles, we determined the ratio of the PM-localized versus intracellular signals by determining gray values in areas of identical size and shape using ImageJ/Fiji software (eight adjacent cells from the epidermis of 6-day-old roots [in the meristematic region] in three different roots were measured and repeated in three biological repeats). The resulting signal ratios were depicted as box plots and their statistical significance was calculated using one-way ANOVA with a post hoc Tukey HSD test. All images of control and chemical-treated samples were taken under the exact same settings of the microscope.

Ubiquitin Binding Assays

Expression of recombinant proteins and *in vitro* binding assays were performed as described by Korbei et al. (2013) and three biological repeats were performed for each experiment. For the ubiquitin binding, equal amounts of di-ubiquitin (linear: BML-UW0775-0100; K48-linked: BML-UW9800-0100; K63-linked: BML-UW0730-0050, from Enzo Life Sciences) were added. For quantification, signal intensities were determined with ImageJ software (http://rsbweb.nih.gov/ij/) and then normalized, with the strongest band randomly being set to 1. Normalized signal intensities are indicated in the figures below blots. Glutathione–Sepharose 4B (GE Healthcare, 17-0756-01) or His Mag Sepharose Ni (GE Healthcare, 28-9673-90) were used.

Pull-Down Assays

Seven-day-old *Arabidopsis* roots (500 mg) expressing TOL2:Ven in *tol2-1* background were shock frozen and ground with a Retsch mill and metal balls. Cold extraction buffer (1 ml; 10% glycerol, 25 mM Tris–HCl [pH 7,4], 1 mM EDTA, 150 mM NaCl, 2% polyvinylpyrrolidone, 1 mM dithioerythritol [DTE], 0,1% Nonidet P-40 [NP-40], and 1× cOmplete Mini Protease Inhibitor Cocktail [Roche]) was added and rotated on a turning wheel (12 rpm) for 30 min at 4°C. After 15 min of centrifugation (20 627 *g*), 1 ml of the soluble root fraction was incubated with recombinant equal amounts of bacterially expressed and purified GST:VPS23A or GST (negative control) (diluted in 400 μl of dilution buffer: 20 mM Tris–HCl [pH 7,4], 5 mM EDTA, 10% glycerol, 1 mM DTE, and 1× cOmplete Mini Protease Inhibitor Cocktail) and rotated on a turning wheel (12 rpm) for 1 h at 4°C. Equilibrated glutathione–Sepharose 4B (60 μl; GE Healthcare; 17-0756-01) was added and rotated on a turning wheel (12 rpm) for 16 h at 4°C. After washing three times with resuspension buffer (20 mM Tris–HCl [pH 7,4], 100 mM NaCl, 1 mM EDTA, 1 mM DTE, and 1× cOmplete Mini Protease Inhibitor Cocktail), bead-bound proteins were eluted with 50 μl of 2× Laemmli buffer (98°C, 10 min) and analyzed by immunoblotting with anti-GFP and anti-GST antibodies.

Immunoprecipitation Experiments

Seven-day-old seedlings (100 mg; Col-0 or *tol6-1*) were shock frozen and ground with a Retsch mill and metal balls. One milliliter of RIPA buffer (50 mM Tris–HCl [pH 7.4], 150 mM NaCl, 1% NP-40, 1% [w/v] sodium deoxycholate, 0.1 % [w/v] SDS, 20 mM NEM, 1× cOmplete Mini Protease Inhibitor Cocktail) was added and incubated for 1 h at 4°C on a Vibrax shaker at 1600 rpm. After 10 min of centrifugation (16 000 *g*, 4°C), 50 μl of affinity-purified TOL6 antibody was added to the supernatant and rotated for 16 h at 4°C on a turning wheel (12 rpm). Protein A magnetic beads (6MB; GE Healthcare) were rehydrated in 1 ml of 1× Tris-buffered saline (TBS) (150 mM NaCl, 20 mM Tris–HCl [pH 7.6]) at 4°C on a turning wheel (12 rpm) for 1 h, followed by three successive washing steps, and the beads were blocked for 12 h on a turning wheel (4°C, 12 rpm) in 1 ml of 1× TBS supplemented with 5% bovine serum albumin (w/v). Sixty microliters of the blocked protein A magnetic beads were added to the cell lysate with TOL6 antibody and rotated for 4 h at 4°C on a turning wheel (12 rpm). The pulled-down protein A beads with the α-TOL6 antibody–TOL6 protein conjugate were washed five times with 1 ml of RIPA buffer. Bead-bound proteins were eluted with 50 μl of 1× Laemmli buffer (98°C, 10 min) and analyzed by immunoblotting with anti-TOL6 and anti-ubq antibodies.

Immunoprecipitation experiments from the soluble or membrane fraction were performed as described by Waidmann et al. (2018), except that fresh NEM (20 mM) was added to the buffer at every step.

ACCESSION NUMBERS

Sequence data from this article can be found in the Arabidopsis Information Resource (TAIR) database under the following accession numbers: *TOL2* (At1g06210), *TOL3* (At1g21380), *TOL5* (At5g63640), *TOL6* (At2g38410), *TOL9* (At4g32760), *VPS23A* (At3g12400), and *UBQ5* (At3g62250).

SUPPLEMENTAL INFORMATION

Supplemental Information is available at *Molecular Plant Online*.

FUNDING

This work has been supported by grants from the Austrian Science Fund (FWF P30850, V 382 Richter-Programm to B.K.; FWF P31493 to C.L.) and by a Doc fellowship from the Austrian Academy of Sciences to L.D.-A.

AUTHOR CONTRIBUTIONS

Conceptualization, C.L. and B.K.; Methodology, J.M.-A., M.S., and B.K; Investigation, J.M.-A., M.S., L.D.-A., C.A., L.J., N.K., and B.K.; Writing – Original Draft, B.K.; Writing – Review & Editing, C.L. and B.K.; Funding Acquisition, C.L., L.D.-A., and B.K.; Supervision, J.M.-A., C.L., and B.K.

ACKNOWLEDGMENTS

We would like to thank Doris Lucyshyn for critically reading the manuscript, Erika Isono for sharing published materials, and Jürgen Kleine-Vehn for valuable comments and discussion. No conflict of interest declared.

Received: September 9, 2019
Revised: January 17, 2020
Accepted: February 13, 2020
Published: February 18, 2020

REFERENCES

Aguilar-Hernandez, V., Kim, D.Y., Stankey, R.J., Scalf, M., Smith, L.M., and Vierstra, R.D. (2017). Mass spectrometric analyses reveal a central role for ubiquitylation in remodeling the *Arabidopsis* proteome during photomorphogenesis. Mol. Plant **10**:846–865.

Bache, K.G., Raiborg, C., Mehlum, A., and Stenmark, H. (2003). STAM and Hrs are subunits of a multivalent ubiquitin-binding complex on early endosomes. J. Biol. Chem. **278**:12513–12521.

Barberon, M., Dubeaux, G., Kolb, C., Isono, E., Zelazny, E., and Vert, G. (2014). Polarization of IRON-REGULATED TRANSPORTER 1

(IRT1) to the plant-soil interface plays crucial role in metal homeostasis. Proc. Natl. Acad. Sci. U S A **111**:8293–8298.

Belda-Palazon, B., Rodriguez, L., Fernandez, M.A., Castillo, M.C., Anderson, E.A., Gao, C., Gonzalez-Guzman, M., Peirats-Llobet, M., Zhao, Q., De Winne, N., et al. (2016). FYVE1/FREE1 interacts with the PYL4 ABA receptor and mediates its delivery to the vacuolar degradation pathway. Plant Cell **28**:2291–2311.

Bilodeau, P.S., Winistorfer, S.C., Allaman, M.M., Surendhran, K., Kearney, W.R., Robertson, A.D., and Piper, R.C. (2004). The GAT domains of clathrin-associated GGA proteins have two ubiquitin binding motifs. J. Biol. Chem. **279**:54808–54816.

Bonifacino, J.S. (2004). The GGA proteins: adaptors on the move. Nat. Rev. Mol. Cell Biol. **5**:23–32.

Cardona-Lopez, X., Cuyas, L., Marin, E., Rajulu, C., Irigoyen, M.L., Gil, E., Puga, M.I., Bligny, R., Nussaume, L., Geldner, N., et al. (2015). ESCRT-III-associated protein ALIX mediates high-affinity phosphate transporter trafficking to maintain phosphate homeostasis in *Arabidopsis*. Plant Cell **27**:2560–2581.

Clague, M.J., and Urbe, S. (2010). Ubiquitin: same molecule, different degradation pathways. Cell **143**:682–685.

Clague, M.J., Urbe, S., and Komander, D. (2019). Breaking the chains: deubiquitylating enzyme specificity begets function. Nat. Rev. Mol. Cell Biol. **20**:338–352.

Clough, S.J., and Bent, A.F. (1998). Floral dip: a simplified method for *Agrobacterium*-mediated transformation of *Arabidopsis thaliana*. Plant J **16**:735–743.

Dettmer, J., Hong-Hermesdorf, A., Stierhof, Y.D., and Schumacher, K. (2006). Vacuolar H^+-ATPase activity is required for endocytic and secretory trafficking in *Arabidopsis*. Plant Cell **18**:715–730.

Dores, M.R., Schnell, J.D., Maldonado-Baez, L., Wendland, B., and Hicke, L. (2010). The function of yeast epsin and Ede1 ubiquitin-binding domains during receptor internalization. Traffic **11**:151–160.

Dubeaux, G., and Vert, G. (2017). Zooming into plant ubiquitin-mediated endocytosis. Curr. Opin. Plant Biol. **40**:56–62.

Erpapazoglou, Z., Walker, O., and Haguenauer-Tsapis, R. (2014). Versatile roles of k63-linked ubiquitin chains in trafficking. Cells **3**:1027–1088.

Fallon, L., Belanger, C.M., Corera, A.T., Kontogiannea, M., Regan-Klapisz, E., Moreau, F., Voortman, J., Haber, M., Rouleau, G., Thorarinsdottir, T., et al. (2006). A regulated interaction with the UIM protein Eps15 implicates parkin in EGF receptor trafficking and PI(3)K-Akt signalling. Nat. Cell Biol. **8**:834–842.

Gao, C., Luo, M., Zhao, Q., Yang, R., Cui, Y., Zeng, Y., Xia, J., and Jiang, L. (2014). A unique plant ESCRT component, FREE1, regulates multivesicular body protein sorting and plant growth. Curr. Biol. **24**:2556–2563.

Gao, C., Zhuang, X., Shen, J., and Jiang, L. (2017). Plant ESCRT complexes: moving beyond endosomal sorting. Trends Plant Sci. **22**:986–998.

Herberth, S., Shahriari, M., Bruderek, M., Hessner, F., Muller, B., Hulskamp, M., and Schellmann, S. (2012). Artificial ubiquitylation is sufficient for sorting of a plasma membrane ATPase to the vacuolar lumen of *Arabidopsis* cells. Planta **236**:63–77.

Hershko, A., and Ciechanover, A. (1998). The ubiquitin system. Annu. Rev. Biochem. **67**:425–479.

Hicke, L., Schubert, H.L., and Hill, C.P. (2005). Ubiquitin-binding domains. Nat. Rev. Mol. Cell Biol. **6**:610–621.

Hoeller, D., Crosetto, N., Blagoev, B., Raiborg, C., Tikkanen, R., Wagner, S., Kowanetz, K., Breitling, R., Mann, M., Stenmark, H., et al. (2006). Regulation of ubiquitin-binding proteins by monoubiquitination. Nat. Cell Biol. **8**:163–169.

Hoeller, D., and Dikic, I. (2010). Regulation of ubiquitin receptors by coupled monoubiquitination. Subcell Biochem. **54**:31–40.

Holstein, S.E., and Oliviusson, P. (2005). Sequence analysis of *Arabidopsis thaliana* E/ANTH-domain-containing proteins: membrane tethers of the clathrin-dependent vesicle budding machinery. Protoplasma **226**:13–21.

Hong, Y.H., Ahn, H.C., Lim, J., Kim, H.M., Ji, H.Y., Lee, S., Kim, J.H., Park, E.Y., Song, H.K., and Lee, B.J. (2009). Identification of a novel ubiquitin binding site of STAM1 VHS domain by NMR spectroscopy. FEBS Lett. **583**:287–292.

Hruz, T., Laule, O., Szabo, G., Wessendorp, F., Bleuler, S., Oertle, L., Widmayer, P., Gruissem, W., and Zimmermann, P. (2008). Genevestigator v3: a reference expression database for the meta-analysis of transcriptomes. Adv. Bioinformatics **2008**:420747.

Hua, Z., and Vierstra, R.D. (2011). The cullin-RING ubiquitin-protein ligases. Annu. Rev. Plant Biol. **62**:299–334.

Hurley, J.H. (2010). The ESCRT complexes. Crit. Rev. Biochem. Mol. Biol. **45**:463–487.

Hurley, J.H., and Hanson, P.I. (2010). Membrane budding and scission by the ESCRT machinery: it's all in the neck. Nat. Rev. Mol. Cell Biol. **11**:556–566.

Husnjak, K., and Dikic, I. (2012). Ubiquitin-binding proteins: decoders of ubiquitin-mediated cellular functions. Annu. Rev. Biochem. **81**:291–322.

Isono, E., and Kalinowska, K. (2017). ESCRT-dependent degradation of ubiquitylated plasma membrane proteins in plants. Curr. Opin. Plant Biol. **40**:49–55.

Johnson, A., and Vert, G. (2016). Unraveling K63 polyubiquitination networks by sensor-based proteomics. Plant Physiol. **171**:1808–1820.

Kalinowska, K., and Isono, E. (2014). Analysis of global ubiquitylation and ubiquitin-binding domains involved in endosomal trafficking. Methods Mol. Biol. **1209**:189–202.

Kalinowska, K., Nagel, M.K., Goodman, K., Cuyas, L., Anzenberger, F., Alkofer, A., Paz-Ares, J., Braun, P., Rubio, V., Otegui, M.S., et al. (2015). *Arabidopsis* ALIX is required for the endosomal localization of the deubiquitinating enzyme AMSH3. Proc. Natl. Acad. Sci. U S A **112**:E5543–E5551.

Kasai, K., Takano, J., Miwa, K., Toyoda, A., and Fujiwara, T. (2011). High boron-induced ubiquitination regulates vacuolar sorting of the BOR1 borate transporter in *Arabidopsis thaliana*. J. Biol. Chem. **286**:6175–6183.

Katzmann, D.J., Stefan, C.J., Babst, M., and Emr, S.D. (2003). Vps27 recruits ESCRT machinery to endosomes during MVB sorting. J. Cell Biol. **162**:413–423.

Kim, D.Y., Scalf, M., Smith, L.M., and Vierstra, R.D. (2013). Advanced proteomic analyses yield a deep catalog of ubiquitylation targets in *Arabidopsis*. Plant Cell **25**:1523–1540.

Kolb, C., Nagel, M.K., Kalinowska, K., Hagmann, J., Ichikawa, M., Anzenberger, F., Alkofer, A., Sato, M.H., Braun, P., and Isono, E. (2015). FYVE1 is essential for vacuole biogenesis and intracellular trafficking in *Arabidopsis*. Plant Physiol. **167**:1361–1373.

Komander, D., and Rape, M. (2012). The ubiquitin code. Annu. Rev. Biochem. **81**:203–229.

Korbei, B., and Luschnig, C. (2013). Plasma membrane protein ubiquitylation and degradation as determinants of positional growth in plants. J. Integr. Plant Biol. **55**:809–823.

Korbei, B., Moulinier-Anzola, J., De-Araujo, L., Lucyshyn, D., Retzer, K., Khan, M.A., and Luschnig, C. (2013). *Arabidopsis* TOL proteins act as gatekeepers for vacuolar sorting of PIN2 plasma membrane protein. Curr. Biol. **23**:2500–2505.

Lange, A., Castaneda, C., Hoeller, D., Lancelin, J.M., Fushman, D., and Walker, O. (2012). Evidence for cooperative and domain-specific binding of the signal transducing adaptor molecule 2 (STAM2) to Lys63-linked diubiquitin. J. Biol. Chem. **287**:18687–18699.

Lauwers, E., Erpapazoglou, Z., Haguenauer-Tsapis, R., and Andre, B. (2010). The ubiquitin code of yeast permease trafficking. Trends Cell Biol. **20**:196–204.

Leitner, J., and Luschnig, C. (2014). Ubiquitylation-mediated control of polar auxin transport: analysis of *Arabidopsis* PIN2 auxin transport protein. Methods Mol. Biol. **1209**:233–249.

Leitner, J., Petrasek, J., Tomanov, K., Retzer, K., Parezova, M., Korbei, B., Bachmair, A., Zazimalova, E., and Luschnig, C. (2012). Lysine63-linked ubiquitylation of PIN2 auxin carrier protein governs hormonally controlled adaptation of *Arabidopsis* root growth. Proc. Natl. Acad. Sci. U S A **109**:8322–8327.

Lohi, O., Poussu, A., Mao, Y., Quiocho, F., and Lehto, V.P. (2002). VHS domain – a longshoreman of vesicle lines. FEBS Lett. **513**:19–23.

MacDonald, C., Buchkovich, N.J., Stringer, D.K., Emr, S.D., and Piper, R.C. (2012). Cargo ubiquitination is essential for multivesicular body intralumenal vesicle formation. EMBO Rep. **13**:331–338.

Martins, S., Dohmann, E.M., Cayrel, A., Johnson, A., Fischer, W., Pojer, F., Satiat-Jeunemaitre, B., Jaillais, Y., Chory, J., Geldner, N., et al. (2015). Internalization and vacuolar targeting of the brassinosteroid hormone receptor BRI1 are regulated by ubiquitination. Nat. Commun. **6**:6151.

Mosesso, N., Nagel, M.K., and Isono, E. (2019). Ubiquitin recognition in endocytic trafficking - with or without ESCRT-0. J. Cell Sci. **132**:jcs232868.

Nagel, M.K., Kalinowska, K., Vogel, K., Reynolds, G.D., Wu, Z., Anzenberger, F., Ichikawa, M., Tsutsumi, C., Sato, M.H., Kuster, B., et al. (2017). *Arabidopsis* SH3P2 is an ubiquitin-binding protein that functions together with ESCRT-I and the deubiquitylating enzyme AMSH3. Proc. Natl. Acad. Sci. U S A **114**:E7197–E7204.

Otegui, M.S. (2018). ESCRT-mediated sorting and intralumenal vesicle concatenation in plants. Biochem. Soc. Trans. **46**:537–545.

Paez Valencia, J., Goodman, K., and Otegui, M.S. (2016). Endocytosis and endosomal trafficking in plants. Annu. Rev. Plant Biol. **67**:309–335.

Piper, R.C., Dikic, I., and Lukacs, G.L. (2014). Ubiquitin-dependent sorting in endocytosis. Cold Spring Harb. Perspect. Biol. **6**. https://doi.org/10.1101/cshperspect.a016808.

Prag, G., Watson, H., Kim, Y.C., Beach, B.M., Ghirlando, R., Hummer, G., Bonifacino, J.S., and Hurley, J.H. (2007). The Vps27/Hse1 complex is a GAT domain-based scaffold for ubiquitin-dependent sorting. Dev. Cell **12**:973–986.

Ren, X., and Hurley, J.H. (2010). VHS domains of ESCRT-0 cooperate in high-avidity binding to polyubiquitinated cargo. EMBO J. **29**:1045–1054.

Romero-Barrios, N., and Vert, G. (2018). Proteasome-independent functions of lysine-63 polyubiquitination in plants. New Phytol. **217**:995–1011.

Row, P.E., Prior, I.A., McCullough, J., Clague, M.J., and Urbe, S. (2006). The ubiquitin isopeptidase UBPY regulates endosomal ubiquitin dynamics and is essential for receptor down-regulation. J. Biol. Chem. **281**:12618–12624.

Sauer, M., and Friml, J. (2014). Plant biology: gatekeepers of the road to protein perdition. Curr. Biol. **24**:R27–R29.

Shen, J.B., Zhao, Q., Wang, X.F., Gao, C.J., Zhu, Y., Zeng, Y.L., and Jiang, L.W. (2018). A plant Bro1 domain protein BRAF regulates multivesicular body biogenesis and membrane protein homeostasis. Nat. Commun. **9**:3784.

Sierra, M.I., Wright, M.H., and Nash, P.D. (2010). AMSH interacts with ESCRT-0 to regulate the stability and trafficking of CXCR4. J. Biol. Chem. **285**:13990–14004.

Sims, J.J., and Cohen, R.E. (2009). Linkage-specific avidity defines the lysine 63-linked polyubiquitin-binding preference of rap80. Mol. Cell **33**:775–783.

Sims, J.J., Haririnia, A., Dickinson, B.C., Fushman, D., and Cohen, R.E. (2009). Avid interactions underlie the Lys63-linked polyubiquitin binding specificities observed for UBA domains. Nat. Struct. Mol. Biol. **16**:883–889.

Spitzer, C., Schellmann, S., Sabovljevic, A., Shahriari, M., Keshavaiah, C., Bechtold, N., Herzog, M., Muller, S., Hanisch, F.G., and Hulskamp, M. (2006). The *Arabidopsis* elch mutant reveals functions of an ESCRT component in cytokinesis. Development **133**:4679–4689.

Stagljar, I., Korostensky, C., Johnsson, N., and te Heesen, S. (1998). A genetic system based on split-ubiquitin for the analysis of interactions between membrane proteins in vivo. Proc. Natl. Acad. Sci. U S A **95**:5187–5192.

Svozil, J., Hirsch-Hoffmann, M., Dudler, R., Gruissem, W., and Baerenfaller, K. (2014). Protein abundance changes and ubiquitylation targets identified after inhibition of the proteasome with syringolin A. Mol. Cell. Proteomics **13**:1523–1536.

Tenno, T., Fujiwara, K., Tochio, H., Iwai, K., Morita, E.H., Hayashi, H., Murata, S., Hiroaki, H., Sato, M., Tanaka, K., et al. (2004). Structural basis for distinct roles of Lys63- and Lys48-linked polyubiquitin chains. Genes Cells **9**:865–875.

Tomanov, K., Luschnig, C., and Bachmair, A. (2014). Ubiquitin Lys 63 chains - second-most abundant, but poorly understood in plants. Front. Plant Sci. **5**:15.

Varadan, R., Assfalg, M., Haririnia, A., Raasi, S., Pickart, C., and Fushman, D. (2004). Solution conformation of Lys63-linked di-ubiquitin chain provides clues to functional diversity of polyubiquitin signaling. J. Biol. Chem. **279**:7055–7063.

Waidmann, S., De-Araujo, L., Kleine-Vehn, J., and Korbei, B. (2018). Immunoprecipitation of membrane proteins from *Arabidopsis thaliana* root tissue. Methods Mol. Biol. **1761**:209–220.

Walton, A., Stes, E., Cybulski, N., Van Bel, M., Inigo, S., Durand, A.N., Timmerman, E., Heyman, J., Pauwels, L., De Veylder, L., et al. (2016). It's time for some "site"-seeing: novel tools to monitor the ubiquitin landscape in *Arabidopsis thaliana*. Plant Cell **28**:6–16.

Wang, H.J., Hsu, Y.W., Guo, C.L., Jane, W.N., Wang, H., Jiang, L., and Jauh, G.Y. (2017). VPS36-dependent multivesicular bodies are critical for plasma membrane protein turnover and vacuolar biogenesis. Plant Physiol. **173**:566–581.

Wang, T., Liu, N.S., Seet, L.F., and Hong, W. (2010). The emerging role of VHS domain-containing Tom1, Tom1L1 and Tom1L2 in membrane trafficking. Traffic **11**:1119–1128.

Weinberg, J.S., and Drubin, D.G. (2014). Regulation of clathrin-mediated endocytosis by dynamic ubiquitination and deubiquitination. Curr. Biol. **24**:951–959.

Winter, V., and Hauser, M.T. (2006). Exploring the ESCRTing machinery in eukaryotes. Trends Plant Sci. **11**:115–123.

Yoshinari, A., Korbei, B., and Takano, J. (2018). TOL proteins mediate vacuolar sorting of the borate transporter BOR1 in *Arabidopsis thaliana*. Soil Sci. Plant Nutr. 1–8.

Zientara-Rytter, K., and Sirko, A. (2016). To deliver or to degrade—an interplay of the ubiquitin-proteasome system, autophagy and vesicular transport in plants. FEBS J. **283**:3534–3555.